UNIVERSITY OF CALIFORNIA
INSTITUTE OF ENGINEERING RESEARCH
BERKELEY, CALIFORNIA

Measurement of Pressures, Forces, and Radiating Waves for Cylinders Oscillating in a Free Surface

by

J. R. Paulling
Robert K. Richardson

Contract Number N-onr-222(30)

SERIES NO. 82
ISSUE NO. 23
DATE June 1962

Measurement of Pressures, Forces, and Radiating Waves for Cylinders Oscillating in a Free Surface

by

J. R. Paulling

Robert K. Richardson

Contract Number N-onr-222(30)

University of California
Institute of Engineering Research
Berkeley 4, California

June, 1962

Abstract

The hydrodynamic problem of a horizontal cylinder of ship-like cross section undergoing heaving oscillations of small amplitude in a free surface has been treated by a number of writers, notably F. Ursell, W. R. Porter, O. Grim, and F. Tasai. However, few experiments have been made to test the results so obtained.

This report describes experiments in which the amplitudes of heave force, pressure at selected girthwise locations, and radiating waves, as well as the phase angles of force and pressure were measured for several heaving cylindrical bodies. These results are compared with theoretical values computed according to Porter's work. Excellent agreement is found between theoretical and measured amplitudes of force and pressure. The agreement for predicted and measured wave heights and for phase angles is substantially good.

The feasibility of obtaining total force by a girthwise integration of measured pressures is shown.

The results and techniques are expected to shed further light on the problem of the response of a ship to a seaway.

TABLE OF CONTENTS

List of Symbols

Symbol	Definition
$\bar{A}$	Wave height ratio
A_w	Waterplane area of model
B	Beam of model
b	Heave damping coefficient
F_T	External force required to sustain heave oscillations
g	Acceleration of gravity
m	Mass of model
m'	Added mass in heave
p	Pressure
s	Coordinate tangential to surface of model section
y_0	Amplitude of heaving motion
$z = x + iy$	Complex coordinate in physical plane
γ	Direction cosine between normal to model surface and y-axis
δ	Non-dimensional frequency
ζ	Complex coordinate in reference plane
η_0	Amplitude of radiating waves at large distance from model
ρ	Mass density of fluid
ϕ, ϕ_p	Phase angle by which force or pressure leads motion
ω	Circular frequency of periodic motion

I. Introduction

The response, either rigid body or elastic, of a ship to the seaway reduces to a problem in the application of Newton's second law to a body, or part of a body, upon which is acting a system of fluid forces and moments together with the weight of the body. The problem is usually simplified by the assumptions of an inviscid, incompressible fluid and small motion. Under the former assumption the fluid forces appear as pressures normal to the hull surface. The time-dependent pressures (and forces), as a result of a linearization of the problem based on the latter assumption, are conveniently divided into two categories: (1) Those dependent on ship geometry and wave motion; (2) Those dependent on ship geometry and ship motion. When one writes the differential equations of ship motion in waves, the former of these assume the role of "exciting" or "forcing" terms on the right hand side of the equations, while the latter appear as functions of displacement, velocity and acceleration on the left-hand side. Note that, under these conditions, the wave-dependent terms are independent of ship motions and thus are the same whether the ship is free to move under their influence or is constrained against such motion. Similarly, the motion-dependent terms are independent of the waves, thus are the same for the ship undergoing identical motions in waves or in calm water.

We observe that a treatment of the rigid-body problem requires the integral of these pressure forces over the entire surface of the ship. The determination of the ship's elastic response requires the pressure distribution.

A typical study of one phase of the rigid-body problem, the motion in the vertical longitudinal plane corresponding to ship operation in ahead or astern seas is given in reference [1]. References [2] and [3] describe the computation of one phase of the elastic problem, the longitudinal hull bending moment in such a seaway. In [1] the author has determined the magnitudes of the motion-dependent total forces and moments by experiment, whereas in [2] and [3], use is made of a "slender-body" assumption with regards to the ship hull, together with theoretical two-dimensional force data. In this latter approximate computation, it is assumed that the flow at each station of the hull is two-dimensional, and, that the hydrodynamic pressures (and force per unit length) will therefore be the same as those on a cylinder of the same section shape undergoing the same vertical motion. The resulting two-dimensional hydrodynamic problem is much more amenable to solution than the complete three-dimensional problem. Theoretical values of force per unit length for a semi-circular cylinder heaving at any frequency are given by Ursell [4]. It is found that, at very high frequencies, the velocity-dependent pressure vanishes leaving only the acceleration-dependent term. The resulting problem is greatly simplified. Results for more general shapes in this limiting case of very high frequencies are given by F. M. Lewis [5] and Landweber and Macagno [6].

More recently, Porter [7] has developed a procedure valid for all frequencies and applicable to a wide class of cylindrical shapes including those given by Lewis in [5] and

Landweber and Macagno in [6]. In addition to total force per unit length, Porter gives the girthwise distribution of pressure around the section and the amplitude of waves generated by the section oscillating in heave. In this reference, results are given for some measurements of heaving force and pressures at three points on a semi-circular cylinder which was forced to oscillate in heave. Aside from some measurements reported by Tasai [8] of the waves generated by oscillating semi-submerged cylinders, this appears to be the only attempt, to date, to experimentally check the theoretically determined forces on cylindrical bodies undergoing forced heaving oscillations.

The dearth of experimental two-dimensional force data is all the more surprising when one considers that a number of investigators have measured such total forces and moments on oscillating three-dimensional shapes [1], [9], [10]. Further, at least one investigator has attempted to measure the longitudinal distribution of these forces using a segmented model [11]. Aside from Porter, no one has, to date, attempted to measure the pressure distribution on such two-or-three-dimensional oscillating semi-submerged bodies.

II. Objective of Present Work

In an attempt to alleviate the noted lack of experimental two-dimensional data, the initial experimental work of Porter has been continued in the Ship Model Tank of the Department of Naval Architecture of the University of California, Berkeley. The immediate objective of this work is to provide substantiation for the two-dimensional computation. Since some of the experimental techniques are new, a major objective is the development and testing of techniques for measuring forces and pressures on small ship models. These two-dimensional studies are considered the first step in a long-range program which has as its ultimate goal, the detailed determination of the force distribution over the envelope of a ship operating in a seaway.

Reported here are measurements of amplitudes and phase angles of pressures at several locations, amplitude and phase angles of total force per unit length, and the amplitude of radiating waves for four cylinders undergoing forced heaving oscillations at a liquid free surface. The total heaving force is obtained in two ways. First, by direct force measurement, and second, by integrating the vertical component of the pressure around the girth of the model. A comparison of the two values so obtained provides a test of the reliability of the measuring apparatus since the two results are essentially independent but simultaneous measurements of the same quantity. In addition, the pressure measurement and integration technique is proposed to be used later in measuring the longitudinal distribution of forces on a

a three-dimensional model. The present work with cylinders provides a test of the feasibility of the method.

These experimental results are compared with similar quantities computed following the procedure of Porter.

III. Experimental Procedure and Apparatus.

The computation assumes a cylinder of infinite length undergoing small sinusoidal heaving oscillations at the free surface of a fluid of unlimited depth. In the laboratory, two-dimensional flow (infinite length of cylinder) is attained by orienting a cylindrical model of finite length at right angles to the length of the long narrow towing tank. The model length is made such that clearances between its ends and the tank walls are the minimum necessary to prevent binding. This model is constrained by a mechanical device to follow a sinusoidal heaving motion of amplitude which is small compared to the dimensions of the cross section of the model. The infinite depth condition is approximated by making the model cross-section dimensions small compared to the water depth and the distance to the tank ends. Figure 1 shows the tank with a cylindrical model in place.

Description of Models

Four sections were chosen for the experiments. Drawings of the sections are shown in Figure 2 and photographs of the actual models in Figure 3. These shapes were selected as typical ship sections embracing a diverse range of geometrical properties. For the theoretical computation, these sections are mapped from a circle by the conformal transformation:

$$z = \zeta + \sum_{n=0}^{N} a_{2n+1} \zeta^{-(2n+1)} . \qquad (1)$$

Table I gives the principal dimensions and the coefficients in the above expression for the four models.

TABLE I

MODEL	HALF-BEAM	HALF-BEAM / DRAFT	SECTIONAL AREA COEF	a_1	a_3	a_5
1. Full form	8 in.	1.00	0.9405	0.0	-0.100	0.0
2. Wide vee	8 in.	0.40	0.700	-0.44762	+0.04446	0.0
3. Narrow vee	4 in.	0.20	0.644	-0.7000	+0.0500	0.0
4. Bulb	4 in.	0.20	0.695	+0.7132	-0.02096	+0.0605

The models are of wooden construction and have brass flanges inserted at positions shown in Figure 2 for the purpose of installing pressure gages.

Motion Generating Apparatus.

The sinusoidal-motion mechanism has been described by Watson [12]. Essentially this device consists of two parallel rods carried in bearings which permit axial motion. Each rod is constrained to follow a sinusoidal axial motion by a Scotch-yoke mechanism. The two cranks driving the Scotch yokes are carried on opposite ends of a common shaft and include provision for adjusting the eccentricity of the cranks, thus the amplitude of motion of the rods. A further feature permits a variation of the phase angle of one crank relative to the other. Thus, with the mechanism oriented in such a way that the two guide rods are vertical, with both cranks in phase and set for the same eccentricity, a heaving motion will be imparted to a model attached to the rods. With a

180° phase difference between the two, a pitching motion (in space coordinates) will be imparted to the model. By rotating the device 90° so that the guide rods are horizontal, yaw and/or sway motion may be imparted to a model.

Provision is included for producing electrical signals proportional to the axial displacement of either guide rod for motion-monitoring purposes.

Figure 4 shows this mechanism installed in the tank for oscillating one of the cylinder models in heave. Figure 5 shows the device removed from the tank with model attached. Figure 6 is a schematic drawing of one end of the mechanism.

Force Dynamometer.

The heave force dynamometer consists essentially of a stiff spring interposed between the guide rods and the model. The spring constant is made sufficiently high that under the imposed loads, the deflection of the spring will be small in comparison to the amplitude of heaving motion. Thus, the model motion is the same as the sinusoidal heave motion of the guide rods within a small error equal to the dynamometer spring deflection. This spring deflection is proportional to the total force applied to the model by the guide rods and is detected by a Statham Instrument Company Model G10B unbonded strain gage.

Physically, the force-measuring device consists of a system of six horizontal leaf springs on each guide rod. The inner ends of the springs are fixed to the lower end of the guide rod, and the outer ends are built into an

aluminum box frame which in turn carries the model on its underside. The springs are so arranged that the mechanism is preferential to vertical motion of the frame relative to the guide rod while strongly opposing relative motion in other directions. The transducer is then arranged to measure this vertical relative motion between the frame and the guide rods, thus the vertical deflection of the leaf springs. A typical spring deflection is of the order 0.001 inch with a motion amplitude of 0.25 inch.

The dynamometer frame may be seen in Figures 4 and 5 and a schematic drawing of the dynamometer is shown in Figure 6.

Pressure transducers.

Statham Instrument Company Model PM 233 TC and PM 222 TC pressure gages were used. These are flush-diaphragm, differential-pressure transducers, the former rated at 0.5 psi difference, and the latter 5 psi difference. Atmospheric pressure is used as reference and the average hydrostatic pressure in each case is balanced out initially in the transducer-bridge monitoring circuit. Thus, the measured quantity is the total periodic variation of pressure about this average hydrostatic value. The former gage was chosen for the initial tests because it appeared to be the smallest commercially available flush mounting gage suitable for the small pressures anticipated. The dimensions of this gage (approximately 3/4 inch diaphragm diameter) dictated the minimum model dimensions to permit its insertion without seriously disturbing fairness of the surface. Note that even with the

relatively large model dimensions used, it proved impossible to mount such a gage in regions of sharp curvature such as the turn of the bilge of Model 1.

During the initial tests it was found that the amplifying equipment had a generous margin of available gain when used in conjunction with the PM 233 TC gages. Accordingly, two of the smaller PM 222 TC gages (1/4 inch face diameter) were acquired. These gages are rated at one-tenth the sensitivity of the larger gages, typical figures being 500 microvolts per volt excitation per psi vs 5000 microvolts per volt per psi for the PM 233 TC. These smaller gages were used in the later tests of the program and, in spite of their lower sensitivity, produced adequate output signals.

Wave probe.

The amplitude of the radiating waveswas measured by an electrical resistance wave probe. This device consists of a probe passing through the water surface and a bare ground wire on the tank bottom. The electrical resistance between the probe and ground is found to vary linearly with the wetted length of the probe. A Wheatstone bridge circuit is used to detect this resistance change.

Monitoring and Recording Equipment.

The force, pressure, wave height, and motion transducer outputs were connected to Brush Instrument Company Model RD-5612-00 combination carrier and D.C. recording amplifiers. These amplifiers provide a supply of 3 volts at a carrier frequency of 2 KC for force, pressure, motion, and wave height

transducer bridge excitation. The output was recorded by a Brush Instruments Model RD-2684-50 8-channel rectilinear chart oscillograph.

During the course of the experiments, it was found that the motion produced by the sinusoidal motion mechanism was contaminated by a high-frequency vibration of small amplitude (typically, 30 cps at about .0001"). The force dynamometer, and, to some extent, the pressure transducers were found to be sensitive to this unwanted signal. To eliminate the resultant noise from the recorded output a simple passive low-pass filter was inserted between the carrier and D.C. sections of the amplifier. Filters having identical phase shifts were used in each channel so that relative phase angles between force or pressure and motion were preserved. Attenuation of the signal by the filters was calibrated as a function of frequency and an appropriate correlation made to the output. A sample data record is shown in Figure 7.

Calibration of Instruments.

The heave-force dynamometer is found to have a natural frequency of the order of 20 to 30 cps depending on the mass of the model attached. The pressure gages have natural frequencies of about 3 to 5 KC. Since all of these natural frequencies are well above the heaving frequencies of interest (0 to 3 cps), static calibration of the transducers suffices for the dynamic range of the tests. Such calibrations were carried out by manually moving the apparatus to a number of successive heave positions above and below the mean position, meanwhile recording the transducer outputs (force and pressure) and noting the exact vertical position. The latter measurement was made using

a machinist's dial indicator calibrated in divisions of .001". A straight line was drawn through the points so obtained and the instrument (pressure gage or force dynamometer) constant read as the slope of this line. Figure 8 shows typical calibration curves for pressure and force transducers. Note that the calibration constants in each case have the dimensions inches per chart division. To convert to psi per chart line for the pressure gages, this constant is multiplied by ρg; to convert the force constant to lbs. per chart line, it is multiplied by $\rho g A_w$.

The wave meter similarly was statically calibrated by moving the probe to successive vertical positions, noting the position and recorder pen deflection. These quantities were then plotted and the slope of the straight line so obtained read as the meter constant.

Calibrations were made at the beginning and end of each day's experiments and the mean of the initial and final calibrations used for the final calculations.

Data Analysis.

From the experimental records (Figure 7) the amplitude of the fluctuating pressure, force and wave height were read as one-half the peak-to-peak excursion of the record. The phase angles by which force or pressure led the motion were read by comparing the zero crossings, i.e. the point midway between peaks, of force or pressure and motion records.

In most cases the amplitude was obtained by reading the average peak-to-peak height for three to five

consecutive cycles. The recorded phase angle was taken as the average for the same cycles. After application of the appropriate transducer and noise filter calibration factors, the results were finally reduced to the form:

pressure:	inches of water
force:	inches of water/A_w
wave height:	feet

Newton's second law for the model being forced in simple harmonic heave motion, $y = y_o \cos \omega t$, may be written:

$$-m\omega^2 y_o \cos \omega t = -\rho g A_w y_o \cos \omega t + b\omega y_o \sin \omega t + m'\omega^2 y_o \cos \omega t + \hat{F}_T \cos(\omega t + \hat{\phi}) \qquad (2)$$

Here:

- b = Damping force coefficient
- m' = Added mass in heave
- $\hat{F}_T$ = Amplitude of force applied to the model by the forcing mechanism.
- $\hat{\phi}$ = phase angle by which this force leads the motion

After rearranging this expression, we obtain:

$$\hat{F}_T \cos(\omega t + \hat{\phi}) = (\rho g A_w - m\omega^2 - m'\omega^2) y_o \cos \omega t - b\omega y_o \sin \omega t \qquad (3)$$

from which, after expanding the left hand side:

$$\left.\begin{aligned} \hat{F}_T \cos \hat{\phi} &= [\rho g A_w - (m + m')\omega^2] y_o \\ \hat{F}_T \sin \hat{\phi} &= b\omega y_o \end{aligned}\right\} \qquad (4)$$

The theoretical force, F_T, given by Porter in [7] assumes that the mass of the model, m, equals the mass of

the displaced water. In the experiment, the model was not necessarily ballasted to float in equilibrium at its mean waterline but was constrained to this waterline by the apparatus. Accordingly, the measured force amplitude and phase angles are corrected to the values corresponding to the theoretical mass by the following expressions:

$$\left.\begin{aligned} F_T &= \left[\left(\hat{F}_T \cos\hat{\phi} - \delta m\,\omega^2 y_0\right)^2 + \left(\hat{F}_T \sin\hat{\phi}\right)^2\right]^{1/2} \\ \tan\phi &= \frac{\hat{F}_T \sin\hat{\phi}}{\hat{F}_T \cos\hat{\phi} - \delta m\,\omega^2 y_0} \end{aligned}\right\} \qquad (5)$$

where F_T = corrected heave-force amplitude

ϕ = corrected phase angle

δm = (Theoretical mass of model)-(actual mass of model)

The experimental results are nondimensionalized as follows:

$$\bar{F} = \frac{F_T}{\rho g A_w y_0} \quad ; \text{ dimensionless heave force}$$

$$\bar{p} = \frac{p}{\rho g y_0} \quad ; \text{ dimensionless pressure}$$

$$\bar{A} = \frac{\eta_0}{y_0} \quad ; \text{ dimensionless wave amplitude}$$

$$\delta = \frac{\omega^2 B}{2g} \quad ; \text{ dimensionless frequency}$$

Integration of pressures.

A principal objective of the experiments was to determine the feasibility of obtaining the total heave force by an integration of the measured girthwise pressure distribution. The measured pressure amplitudes were integrated

around the section by the following procedure. Referring to Figure 9, the vertical component of pressure force on a section element, ds, of unit length normal to the figure is:

$$dF = p\,ds\cos\gamma$$

The total vertical pressure force per unit length of section is then

$$F = 2\int_0^{\$} p\cos\gamma\, ds$$

This integral must be evaluated separately for the component of pressure in-phase with the motion and the quadrature component. Thus, if ϕ_p is the phase angle by which pressure leads the motion, the following equations for total force, F_T, and the phase angle of the total force, ϕ, are obtained:

$$\left.\begin{aligned} F_T &= \left[\left(\int_0^{\$} p\cos\gamma\cos\phi_p\, ds - m\omega^2 y_0\right)^2 + \left(\int_0^{\$} p\cos\gamma\sin\phi_p\, ds\right)^2\right]^{1/2} \\ \tan\phi &= \frac{\int_0^{\$} p\cos\gamma\sin\phi_p\, ds}{\int_0^{\$} p\cos\gamma\cos\phi_p\, ds - m\omega^2 y_0} \end{aligned}\right\} \quad (6)$$

In practice, $p\cos\gamma\cos\phi_p$ and $p\cos\gamma\sin\phi_p$ were plotted vs s, a fair curve drawn through the points, and the integral approximated by Simpson's rule or by a planimeter. This procedure was repeated for a number of different values of δ. The value assumed for m in Equation (6) was the mass of the displaced water to correspond with Porter's results.

IV. Results

Experimental results are presented in the form of graphs of $\bar{F}$, $\bar{p}$, $\bar{A}$, ϕ and ϕ_p vs δ. Theoretical values obtained following the method of Porter are plotted on the same graph in each case. The pressures and pressure phase angles are designated by gage location as shown in Figure 2. In several cases, the experiments were repeated for several amplitudes of heave motion. Experimental points corresponding to these different amplitudes are noted by different symbols on the appropriate graph.

Figures 10 through 13 give the amplitude of the measured total force and Figures 22 through 25, the corresponding phase angles. The total force, $\bar{F}$, obtained by integration of the measured pressures are shown for each of the models in Figures 30 through 33, and the corresponding phase angles in Figures 34 - 37.

The measured individual pressures, $\bar{p}$, are plotted vs δ in Figures 14 - 17 and the corresponding phase angles, ϕ_p, by which the pressure leads the motion, in Figures 26 - 29.

Finally, the amplitude of radiating waves, $\bar{A}$, generated by the model is shown for each of the four models in Figures 18 - 21.

Discussion of Results

The reliability of the measurements is illustrated by a

comparison of the total force amplitude from two independent measurements. Referring to the two sets of results, Figures 10-13 and Figures 30-33, we see that the total force as measured directly agrees substantially with that obtained by integration of the measured pressures. In addition, as may be seen in Figures 22-25 and Figures 34-37, the phase angles by which this force leads the motion show the same agreement.

Since the two measurements are completely independent of each other, it is concluded that both accurately measure the quantity in question and that the measuring devices and circuits are free of systematic errors.

In general, the force and phase angle obtained by pressure integration agree somewhat more closely with theoretical values than do the force and phase angle obtained by direct measurement. The low natural frequency of the direct force dynamometer and consequent more severe contamination of the resulting records by vibration offer some explanations for this poorer agreement. During the data reduction, considerably more difficulty was experienced in reading amplitudes and phase angles from these force records than from the pressure records.

Quantitative assessment of total experimental errors is quite difficult because of the many sources present in each measurement. The principal sources of error are thought to

be: (1) Vibration which is not entirely attenuated by the filters in the electronic circuit. The effect on the final results is largely unpredictable since it depends on the reader's judgement in fairing in a mean curve by eye when reading data. (2) Errors in calibration of the filters, approximately 0.5% in amplitude and 3^{o} in phase angle. (3) Error in calibration. From a comparison of force and pressure calibration constants at the beginning and end of each day's tests this error is probably less than 2% in measured amplitudes. (4) Error in the amplitude of motion: approximately 0.001" in 0.250 or 1/4%. (5) Error in the wave-height measurement. Somewhat indeterminate but estimated to be of the order of 10% because of the relatively small measured wave height.

The cumulative error from sources (1) thru (4) is probably less than 5% in the measured amplitudes and at worst 10^{o} in phase angle. These values are consistent with the scatter of experimental points. The wave height measurement shows the poorest agreement with theory and a satisfactory explanation has not been obtained. Since the wave probe was located some distance from the model (See Figure 1) a possible explanation for the discrepancy between measured and theoretically predicted wave heights is attenuation of the wave by viscosity. The effect of viscosity was estimated using results given by Wehausen[13].

For model 1, the calculated height of the wave at the position of the wave probe in the real fluid (water) as compared to the wave height in an inviscid fluid is shown in Table II:

TABLE II

δ	$\frac{\bar{A}_{\text{real fluid}}}{\bar{A}_{\text{inviscid fluid}}}$
3	.948
4	.902

Thus it is seen that the predicted reduction in wave height attributable to viscosity is not as great as the discrepancy between measured wave height and that predicted for a perfect fluid in most cases.

Because of the systematic trend of the wave height measurements for each test condition, it is the feeling of the writers that the error is most probably one of calibration of the wave probe.

Some scatter of experimental points is noted at low frequency. This scatter results from low frequency waves reflecting from the tank ends and returning to the test apparatus after relatively few cycles of motion. For higher frequencies, steady state was attained and the measurements taken before such reflections would return.

V. Conclusions

The following objectives of the investigation have been satisfied:

(1) The sinusoidal motion apparatus and associated force and pressure measuring systems have been shown to operate satisfactorily.

(2) The feasibility of obtaining the hydrodynamic force on a section by an integration of measured pressures has been demonstrated.

(3) Additional substantiation for the theoretically predicted forces, pressures, phase angles, and wave heights given by Porter [7] has been provided. In particular, the approach based on the linearized boundary conditions is further supported.

(4) The lack of experimental information on hydrodynamic forces for oscillating cylinders noted by Ursell [4] has been, at least in part, alleviated.

(5) A vast amount of experience with the equipment and measurement techniques has been gained by all concerned. This is expected to prove of value in future experiments in which similar techniques will be applied to three-dimensional forms.

Acknowledgments

The writers gratefully acknowledge the assistance of Mr. Choung Mook Lee, graduate student in Naval Architecture, and Mr. Norman D. Turner of the Towing Tank Staff in conducting experiments and reducing data. The theoretical data shown on the graphs with experimental results were supplied by Cdr.W. R. Porter, USN. His assistance in freely making available these results is greatly appreciated.

References

[1] Gerritsma, J., "Shipmotions in Longitudinal Waves", International Shipbuilding Progress, Vol. 7, No. 66, Feb. 1960, pp. 49-71.

[2] Jacobs, W. R., "The Analytical Calculations of Ship Bending Moments in Regular Waves", Journal of Ship Research, Vol. 2, No. 1, June 1958, pp. 20-29.

[3] Fay, J. A., "The Motions and Internal Reactions of a Vessel in Regular Waves", Journal of Ship Research, Vol. 1, No. 4, Mar. 1958, pp. 5-14.

[4] Ursell, F., "On the Heaving Motion of a Circular Cylinder on the Surface of a Fluid", Quarterly Journal of Applied Mathematics, Vol. 2, 1949, pp. 218-231.

[5] Lewis, F. M., "The Inertia of the Water Surrounding a Vibrating Ship", Transactions, the Society of Naval Architects and Marine Engineers, Vol. 37, 1929, pp. 1-20.

[6] Landweber, L. and Macagno, M., "Added Mass of Two-dimensional Forms Oscillating in a Free Surface", Journal of Ship Research, Vol. 1, No. 3, Nov. 1957, pp. 20-30.

[7] Porter, W. R., "Pressure Distribution, Added Mass, and Damping Coefficients for Cylinders Oscillating in a Free Surface", University of California IER Report Series 82, Issue 16, July 1960.

[8] Tasai, F., "Measurement of the Wave Height Produced by the Forced Heaving of the Cylinders", Reports of Research Institute for Applied Mechanics, Kyushu University, Fukuoko, Japan, Vol. VIII, No. 29, 1960.

[9] Golovato, P., "The Forces and Moments on a Heaving Surface Ship", Journal of Ship Research, Vol. 1, No. 1, April 1957, pp. 19-26.

[10] Haskind, M.D., and Riman, I.S., "A Method of Determining the Pitching and Heaving Characteristics of Ships" DTMB Translation 253, Feb. 1955.

(References Cont'd)

[11] Bottaccini, M. R., and Schulz, E. F., "Longitudinal Distribution of Added Mass, Virtual Moment of Inertia, Damping Force, and Damping Moment on a Pitching and Heaving Ship", Colorado State University Research Foundation, Civil Engineering Section, Report CER 60 EFS 32, Sept. 1960.

[12] Watson, T. C., "Experimental Investigation of the Vertical Forces Acting on Prolate Spheroids in Sinusoidal Heave Motion", University of California IER Report Series 82, Issue 18, April 1961.

[13] Gertler, M. "The DTMB Planar Motion Mechanism". Paper presented at the Symposium on Towing Tank Facilities, Instrumentation, and Measuring Techniques, Zagreb, Yugoslavia, Sept. 1959.

[14] Wehausen, J. V. "Surface Waves" Vol. IX, Handbuch der Physik, Springer-Verlag, Berlin, 1960.

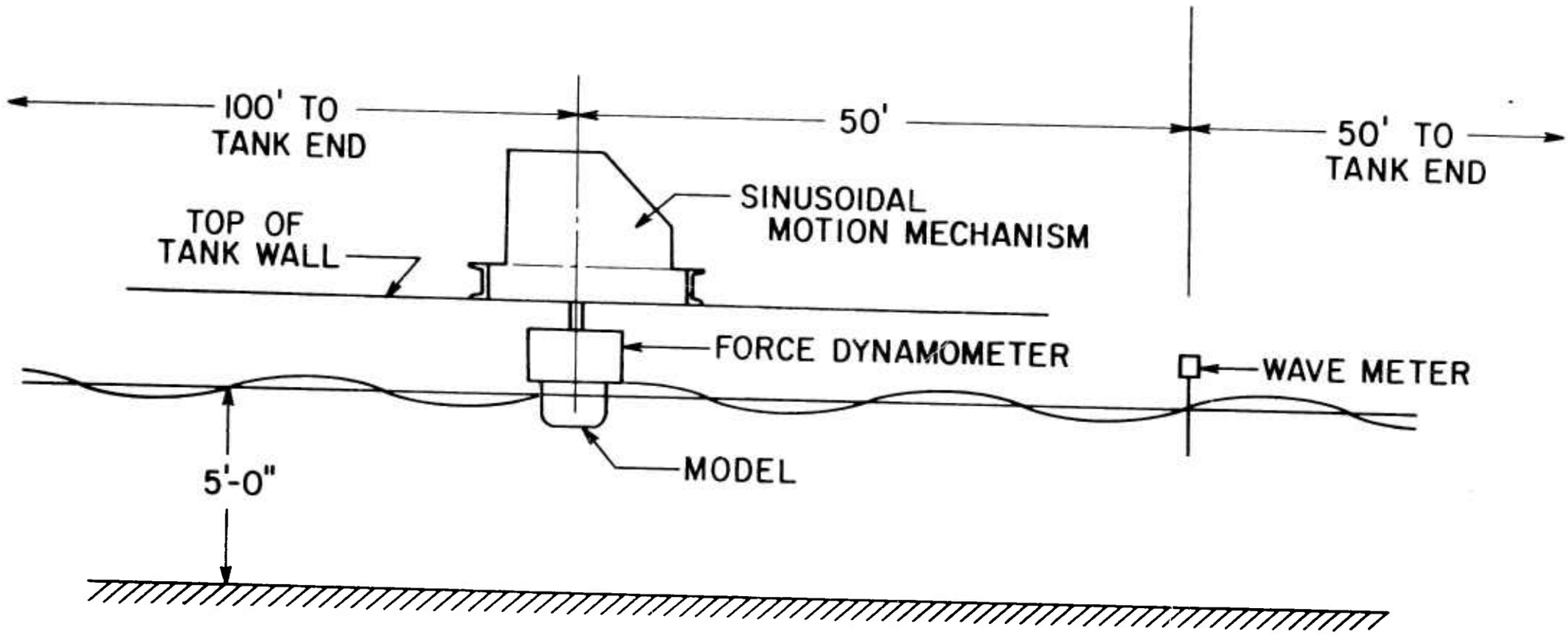

FIG. 1 LONGITUDINAL SECTION OF TANK SHOWING MODEL IN PLACE

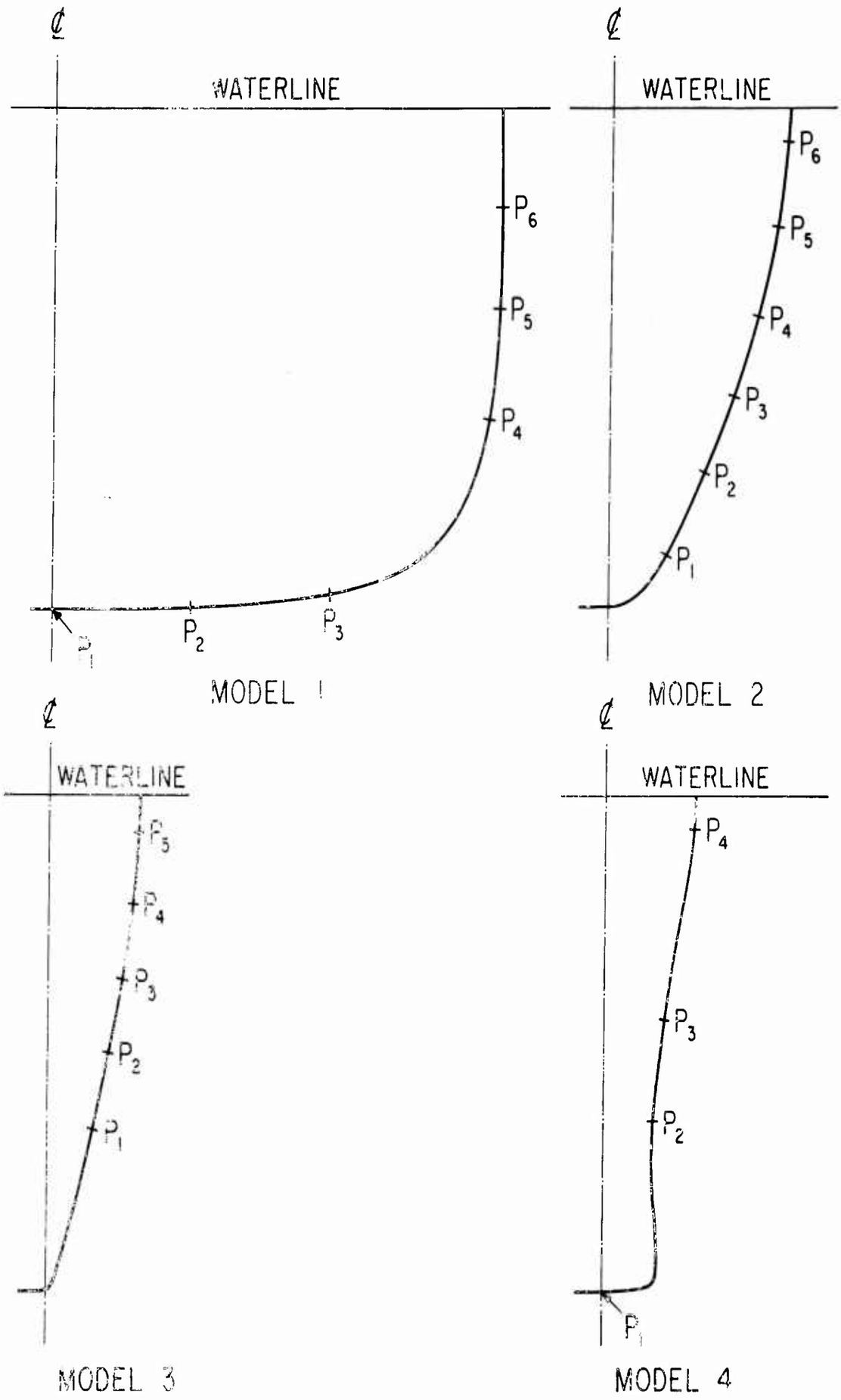

FIG. 2 SECTIONS OF MODELS SHOWING PRESSURE GAGE LOCATIONS

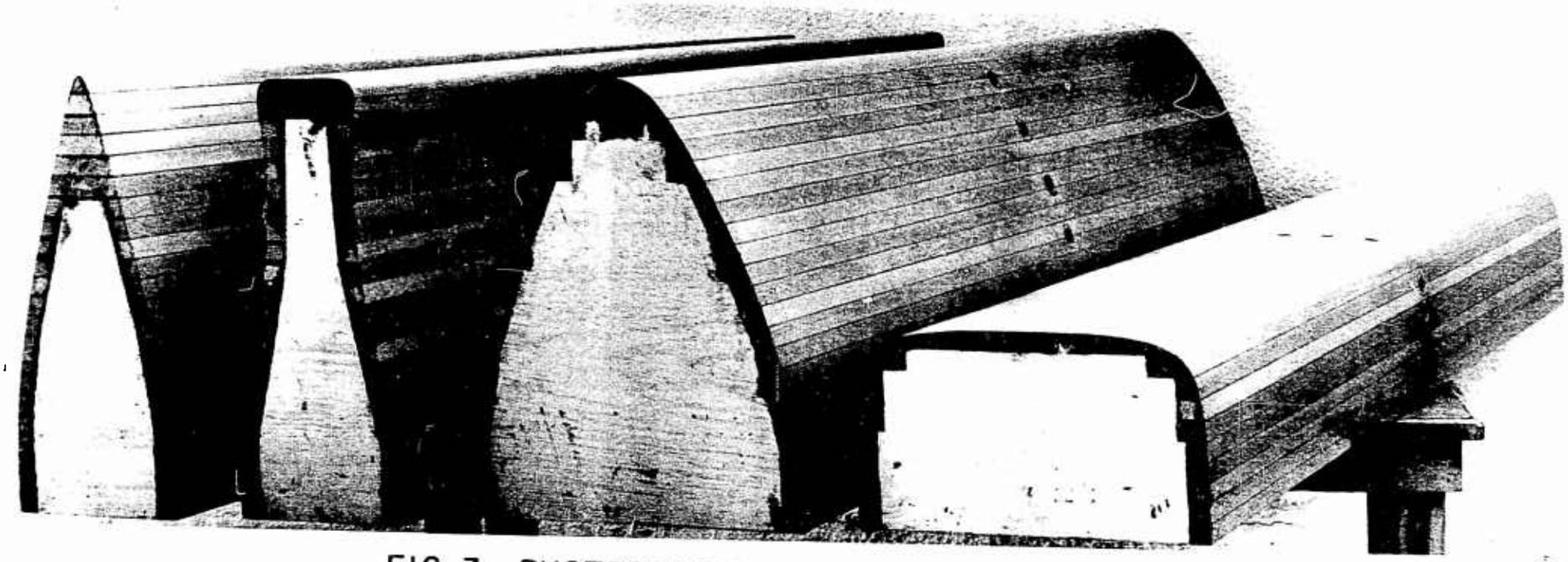

FIG. 3 PHOTOGRAPHS OF CYLINDER MODELS

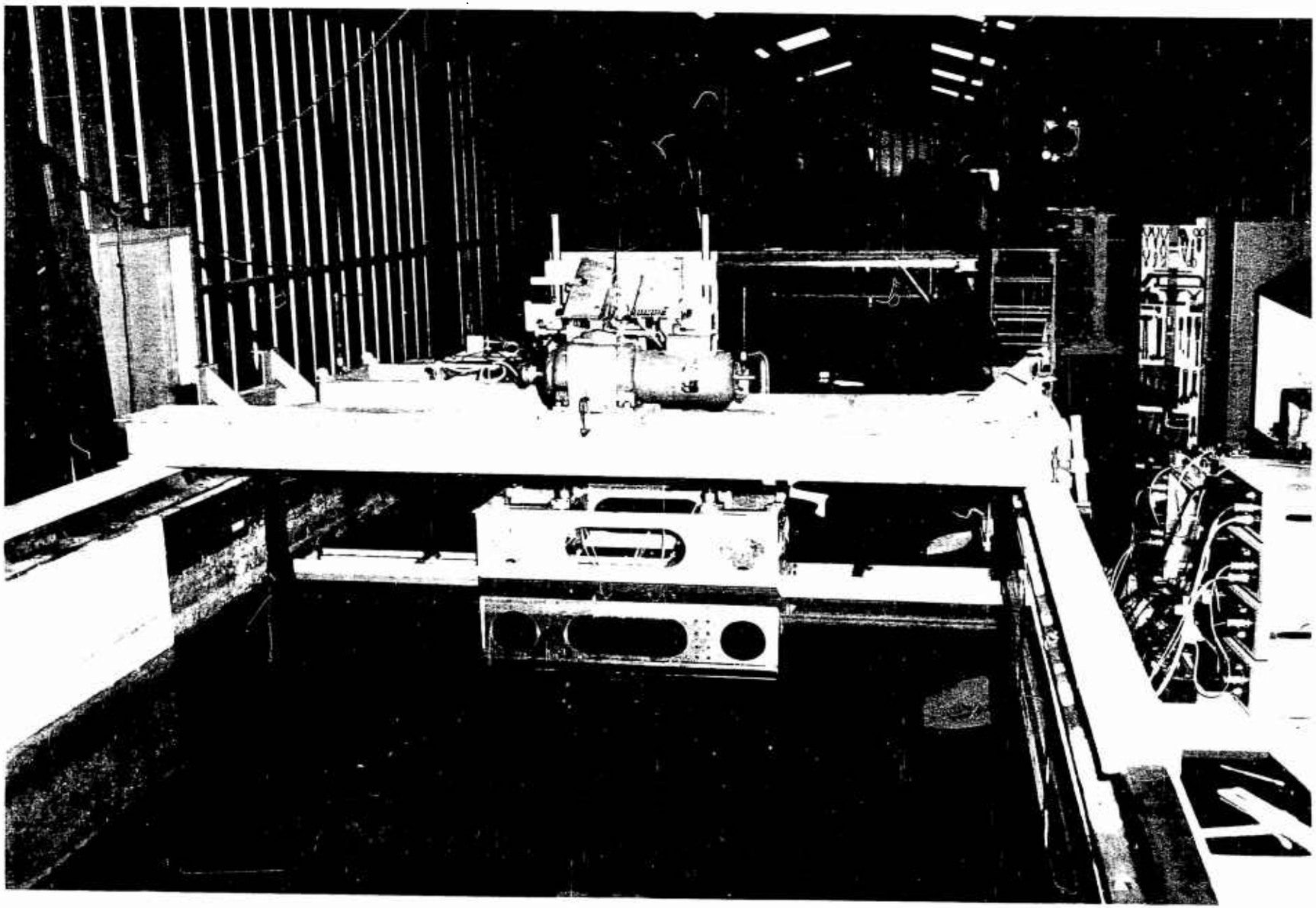

FIG. 4 PHOTOGRAPH OF MOTION GENERATOR AND MODEL IN PLACE IN TANK

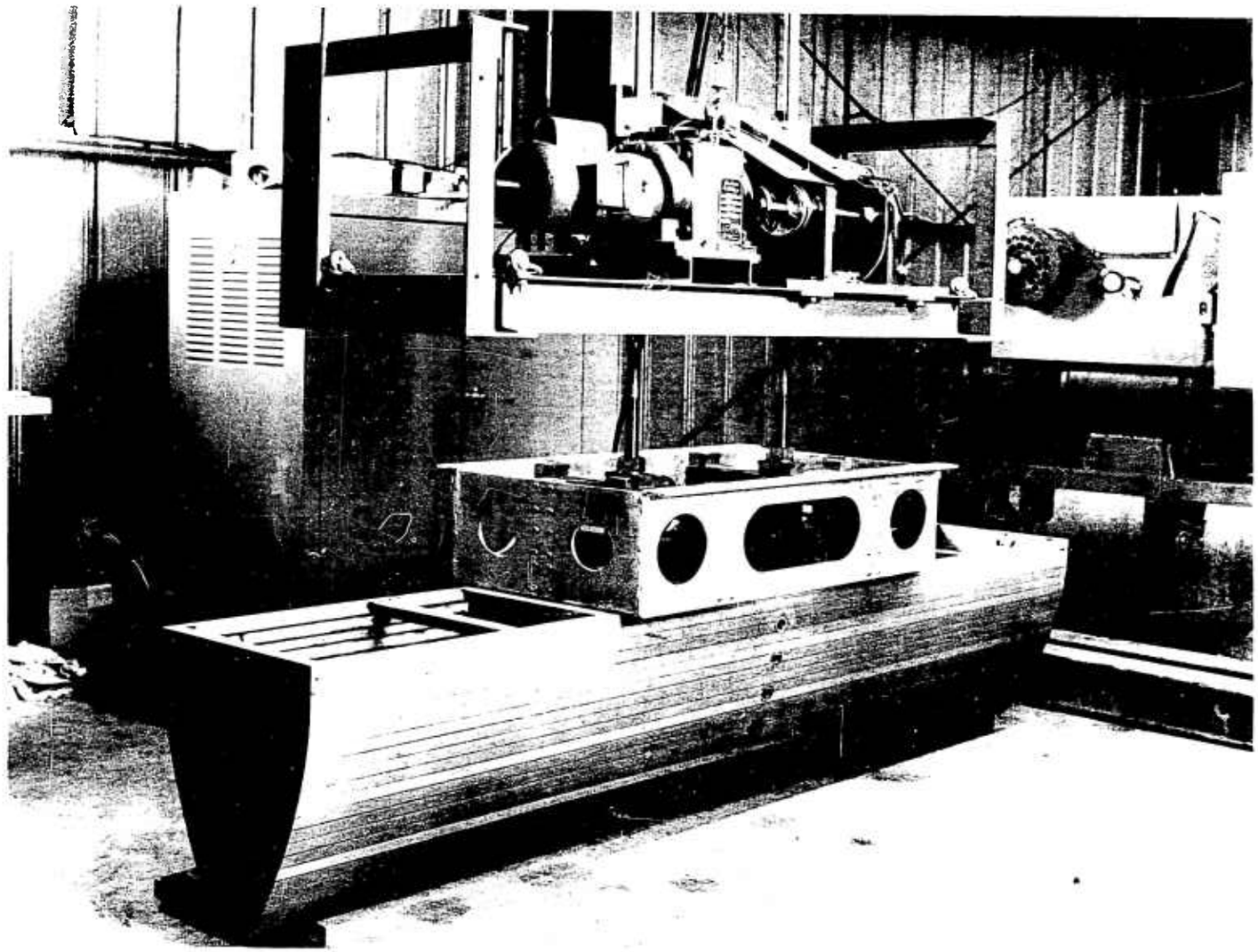

FIG. 5 SINUSOIDAL MOTION MECHANISM AND MODEL REMOVED FROM TANK

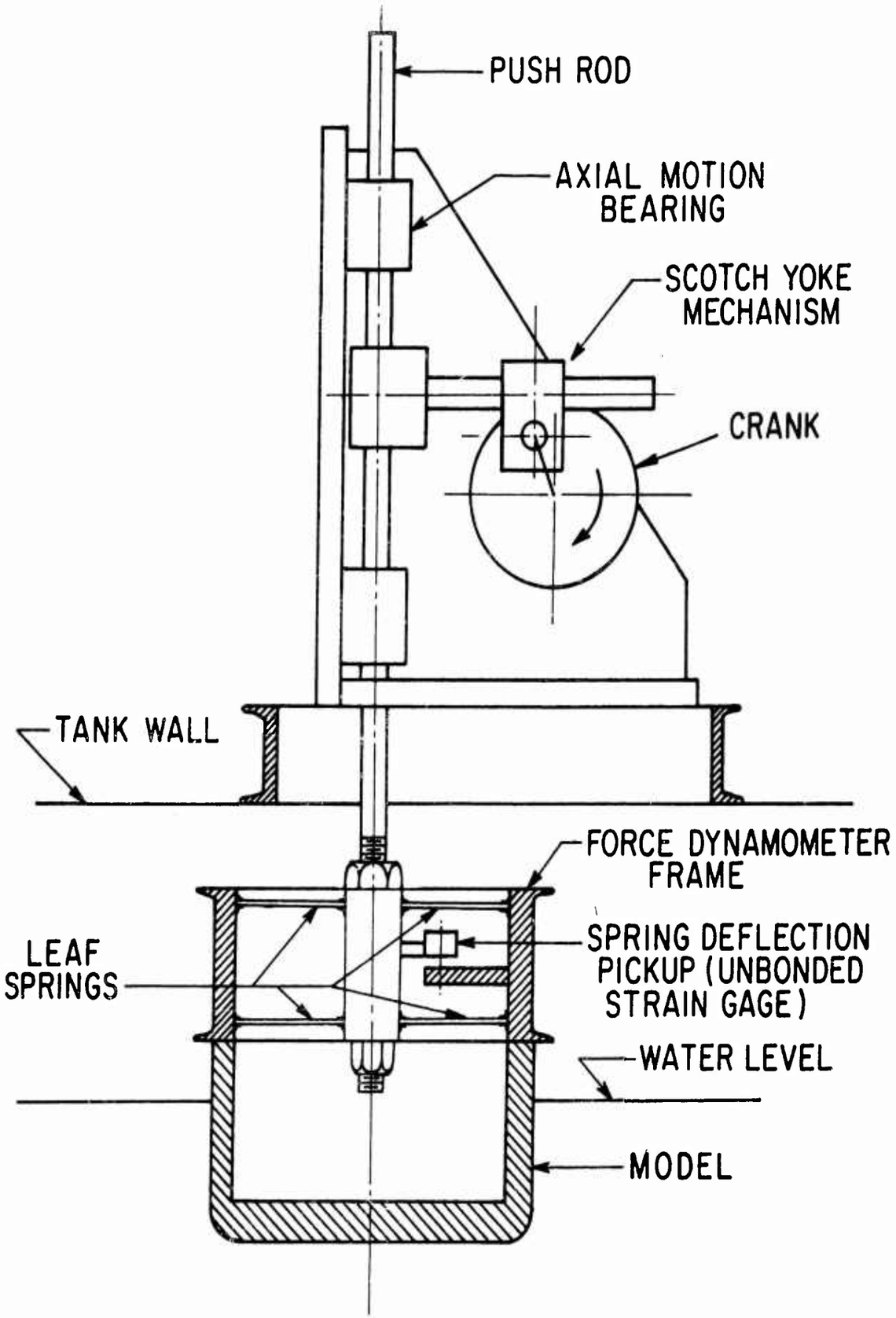

FIG. 6 SCHEMATIC DRAWING OF MOTION GENERATOR AND FORCE DYNAMOMETER

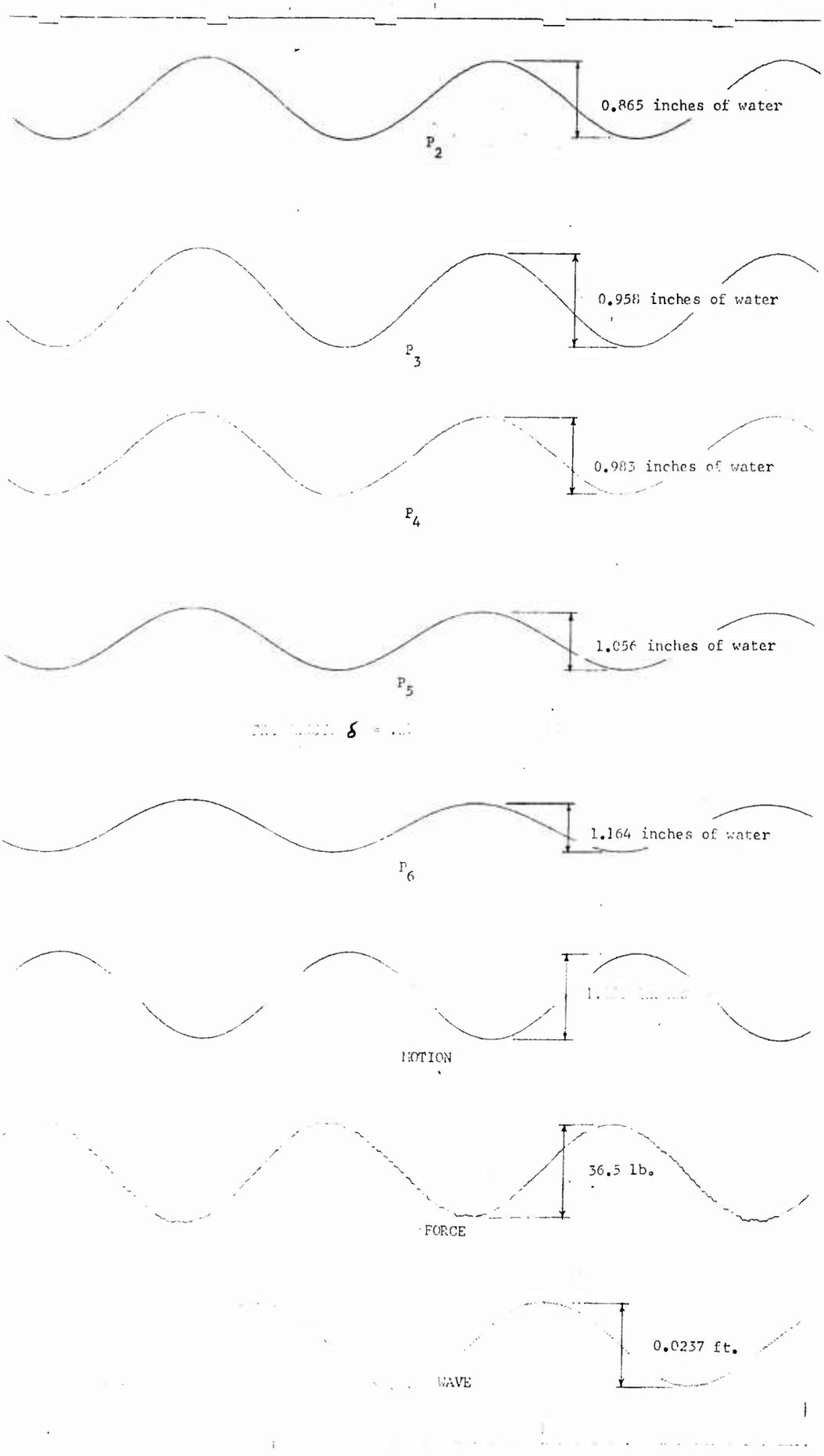

FIG 7 TYPICAL EXPERIMENTAL RECORD
MODEL 2, AMPLITUDE OF MOTION, 1/2" INCH

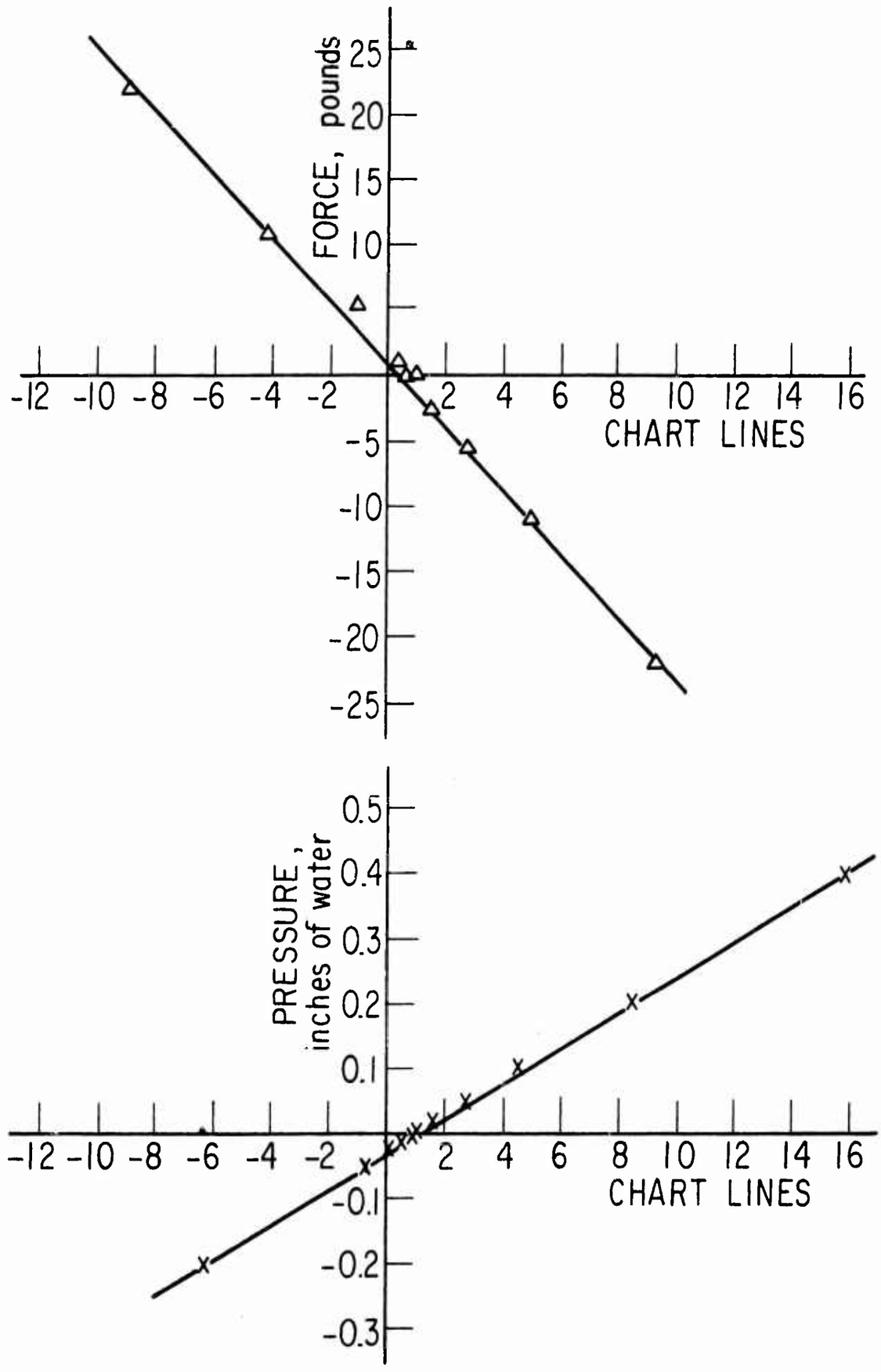

FIG. 8 TYPICAL FORCE METER AND PRESSURE GAGE CALIBRATION

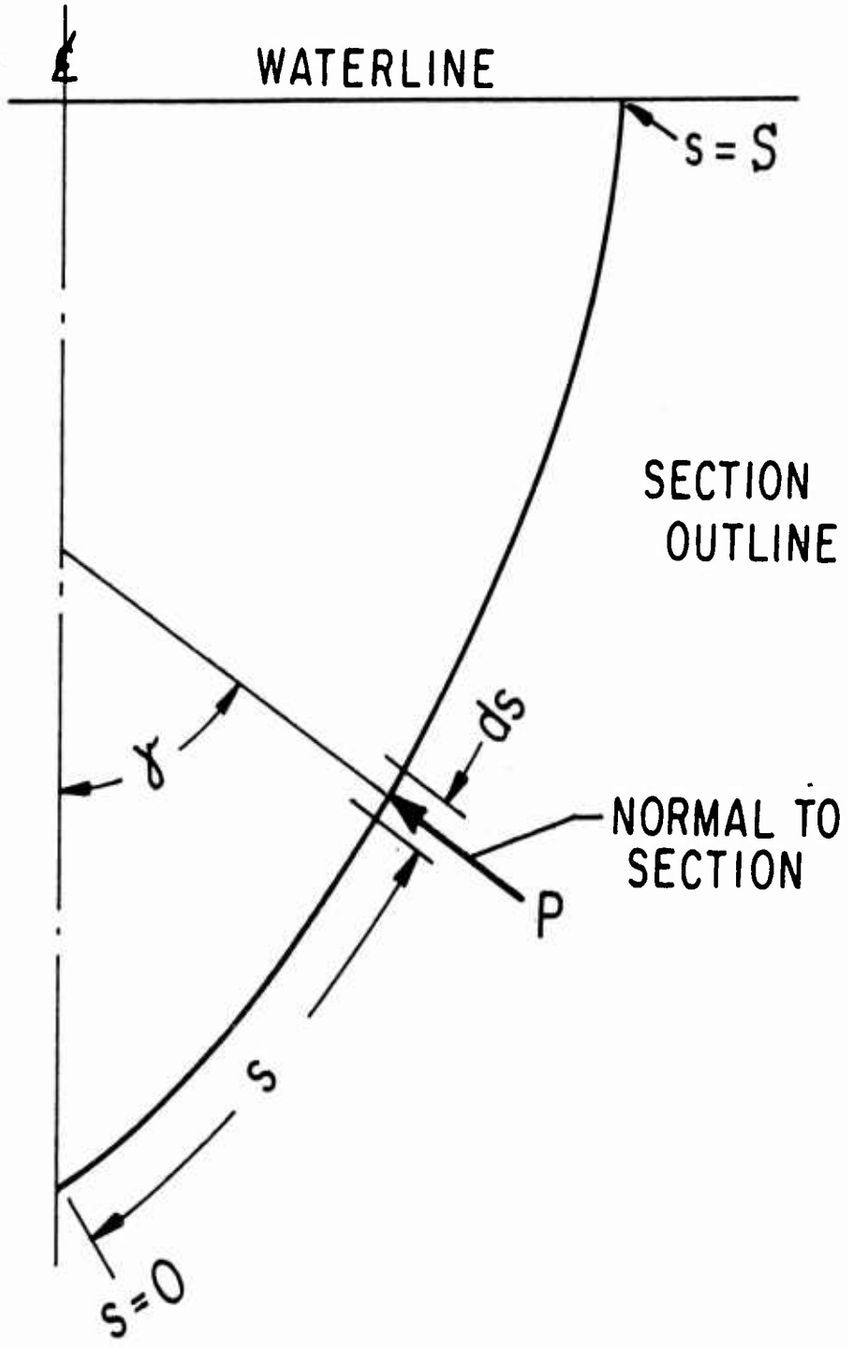

FIG. 9 SKETCH OF MODEL SECTION SHOWING INTEGRATION OF PRESSURE AROUND GIRTH

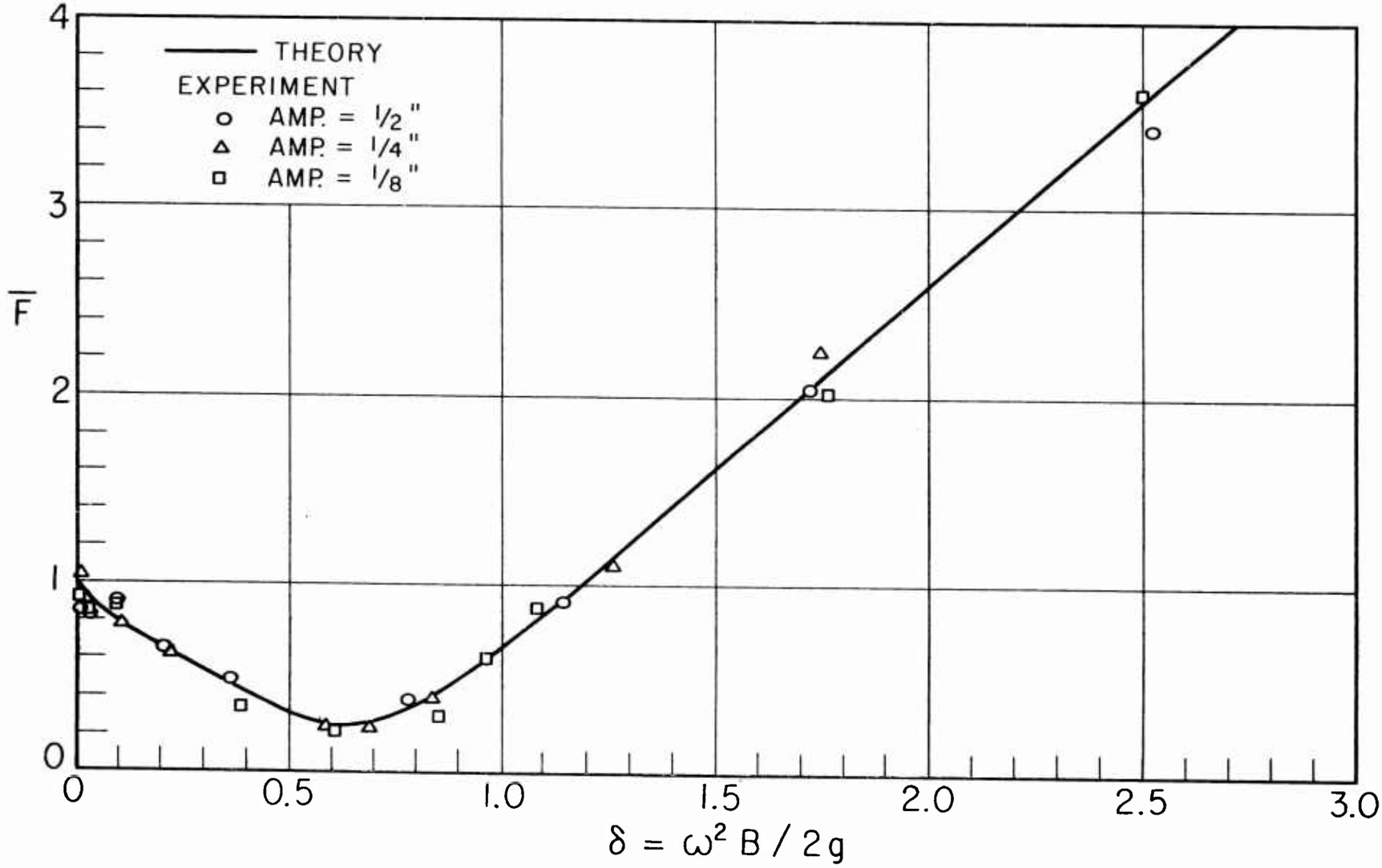

FIG. 10 $\overline{F}$ vs δ FOR MODEL 1

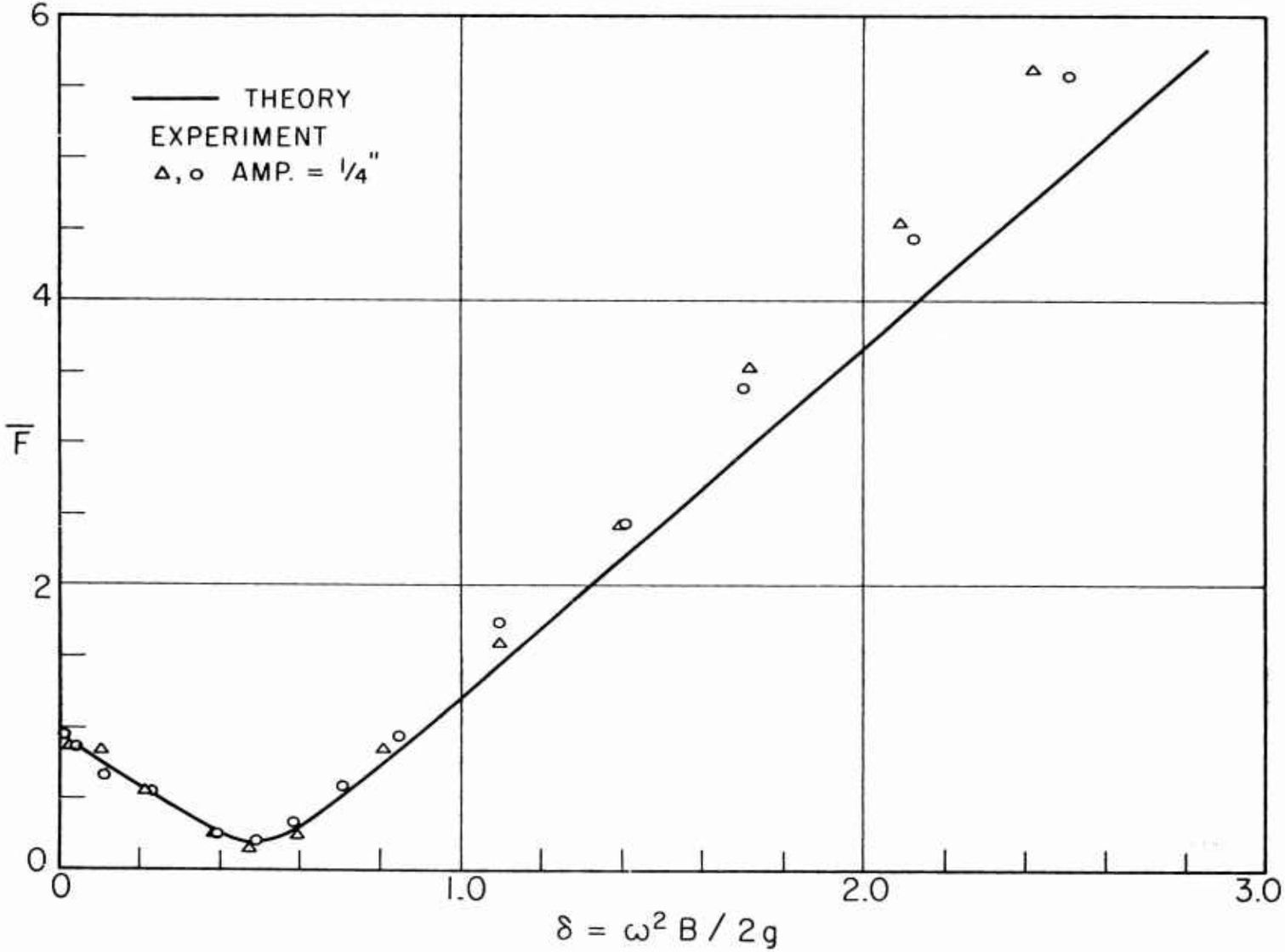

FIG. 11 $\overline{F}$ vs δ FOR MODEL 2

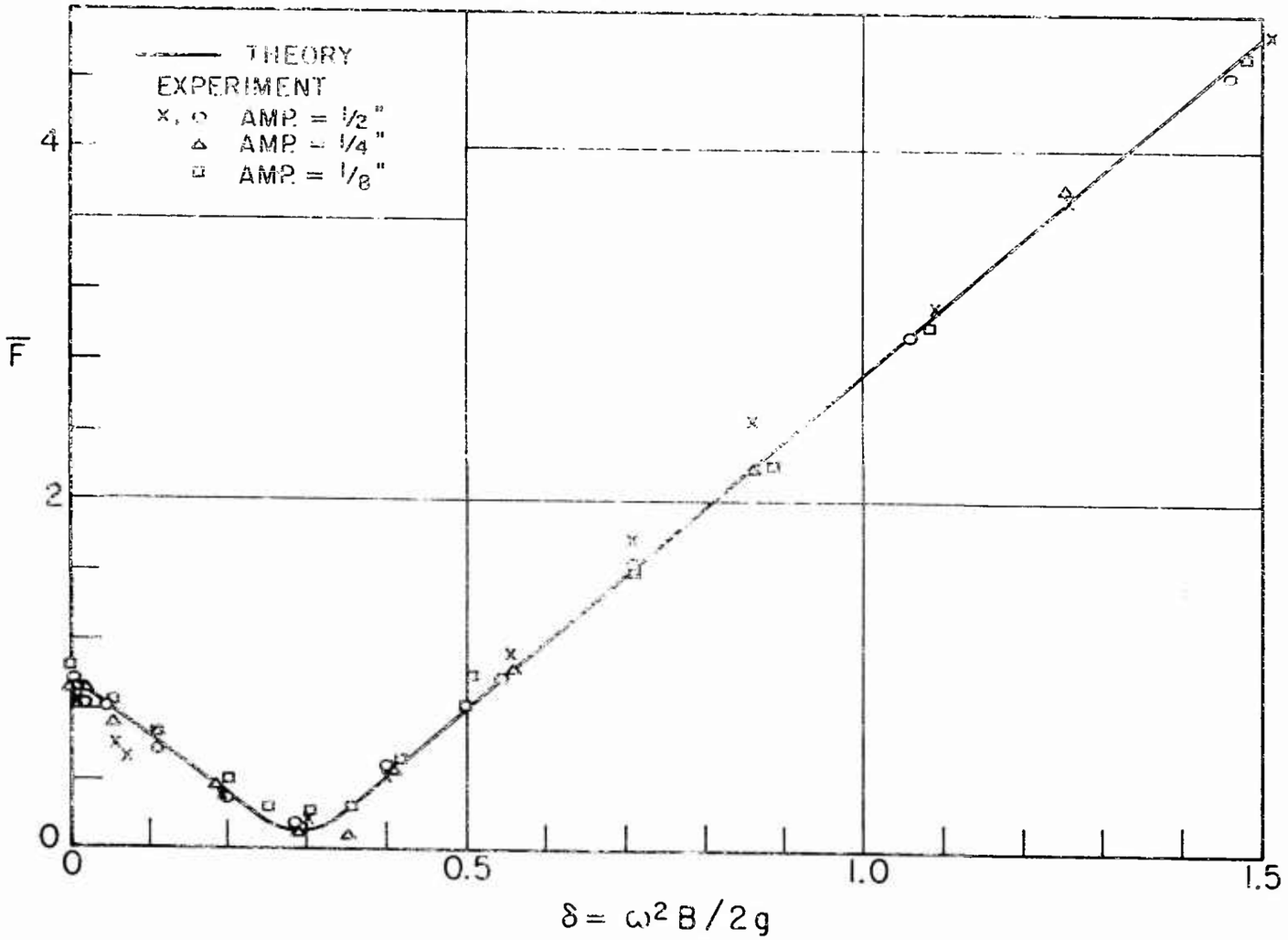

FIG. 12 $\overline{F}$ vs δ FOR MODEL 3

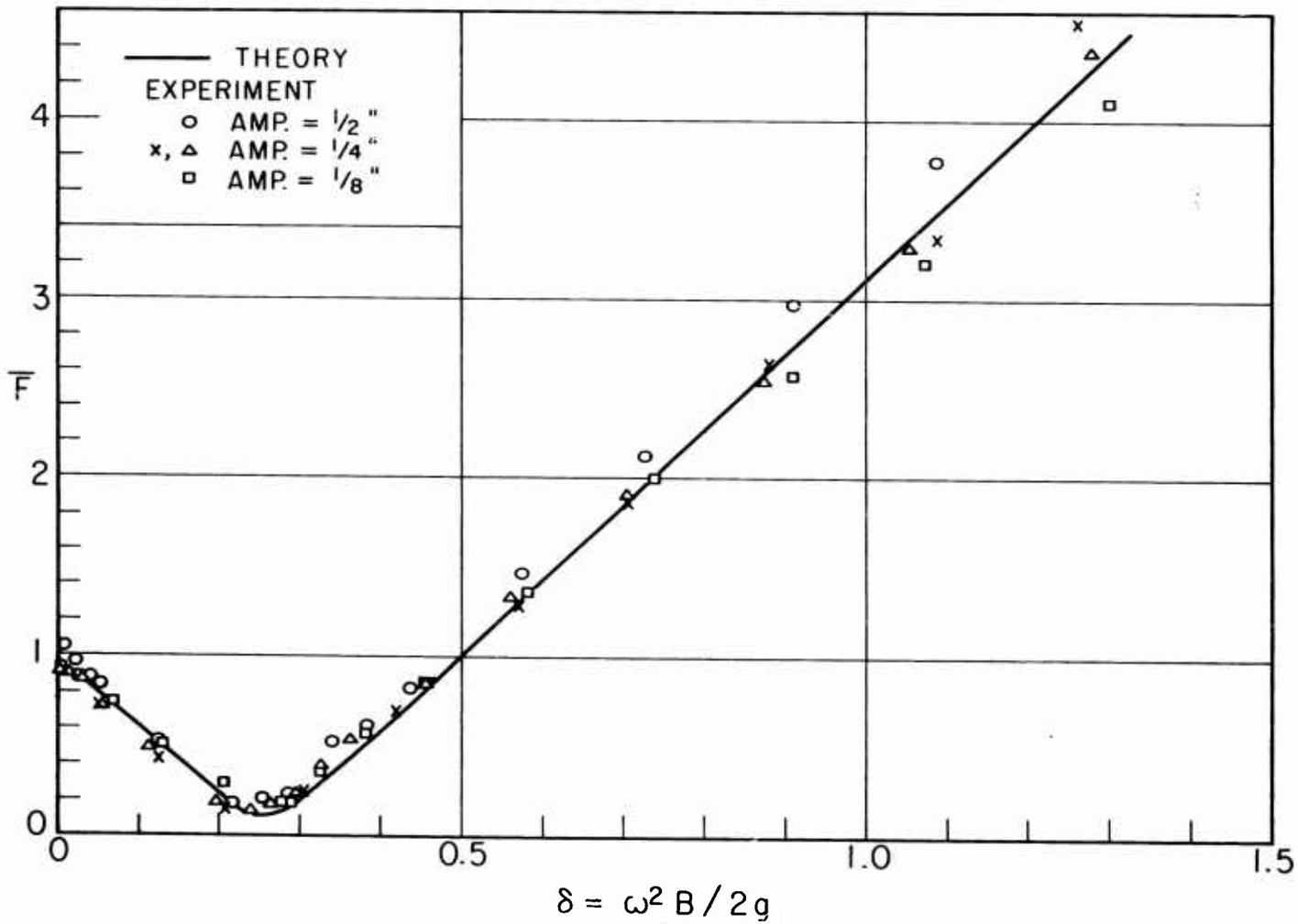

FIG. 13 $\overline{F}$ vs δ FOR MODEL 4

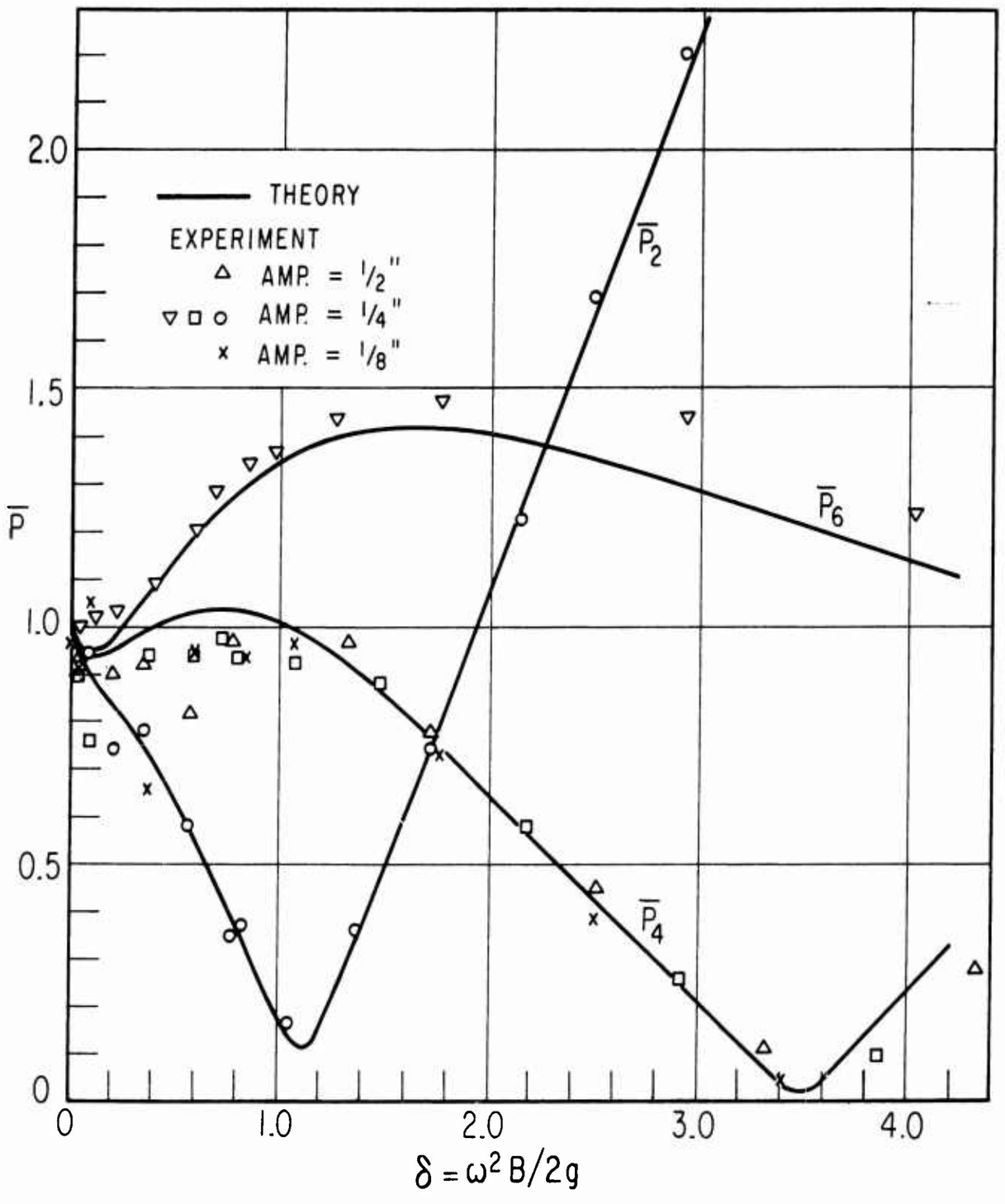

FIG. 14a $\overline{P}$ vs δ FOR MODEL 1

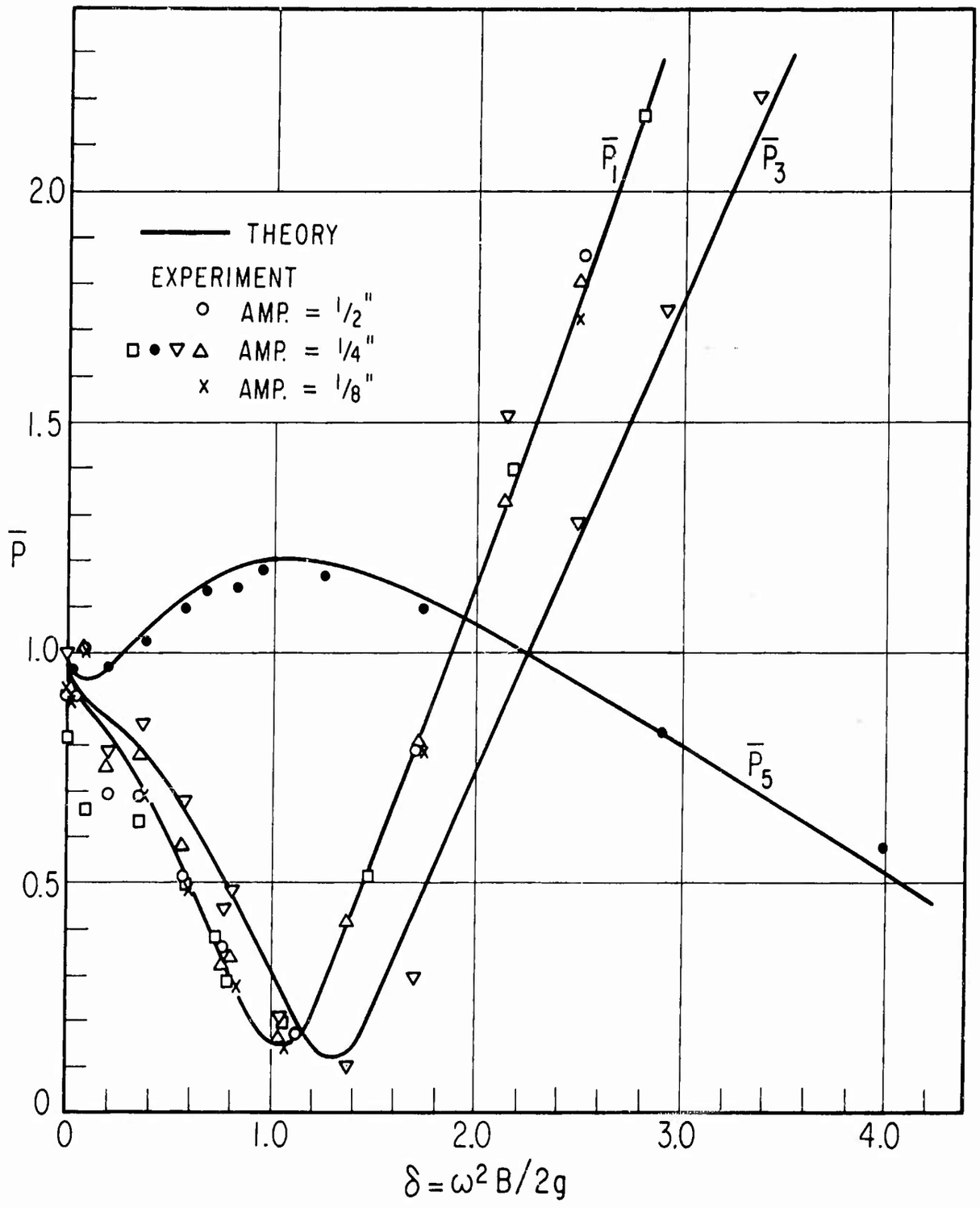

FIG. 14b $\bar{P}$ vs δ FOR MODEL 1

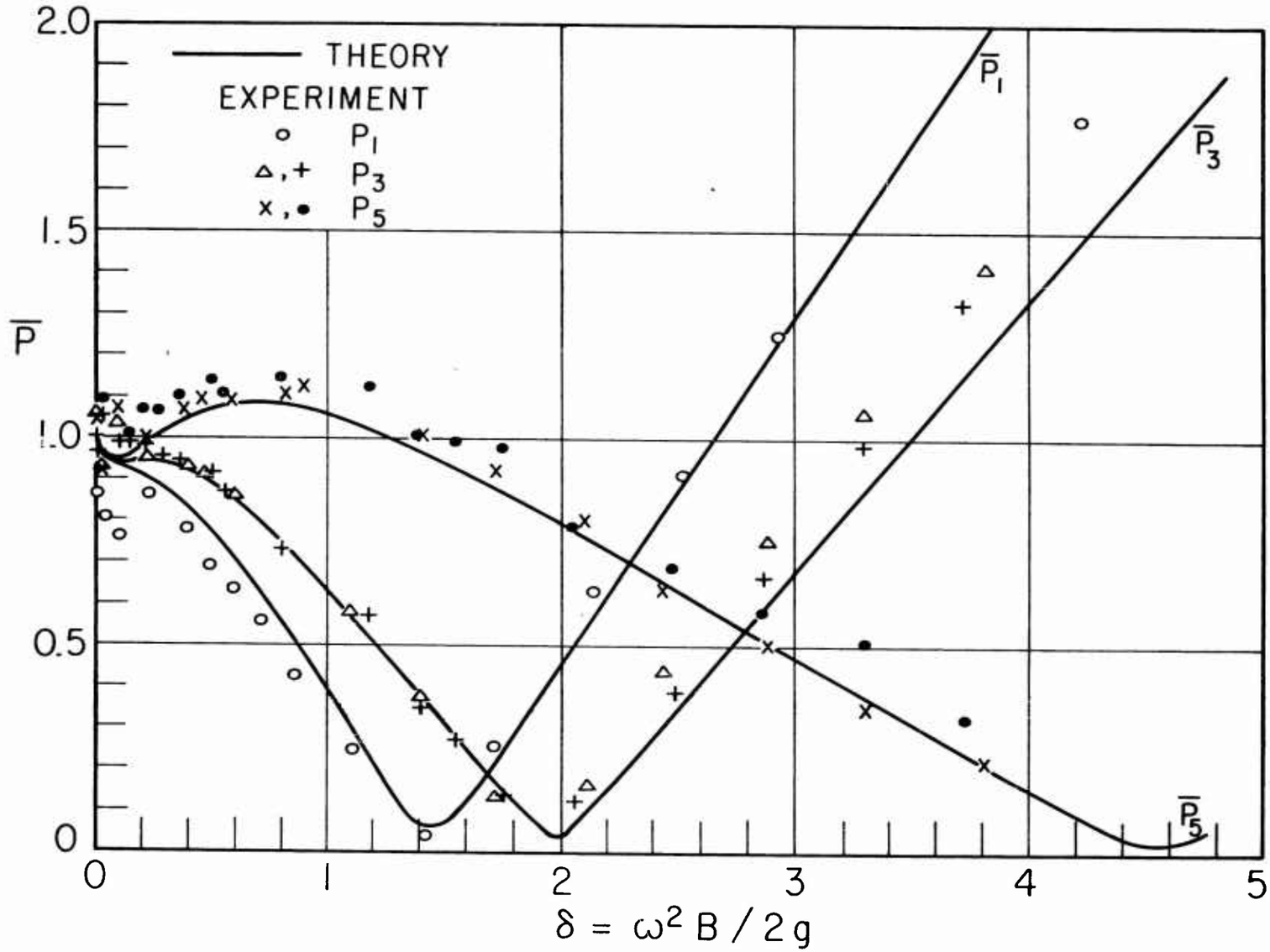

FIG. 15a $\overline{P}$ vs δ FOR MODEL 2

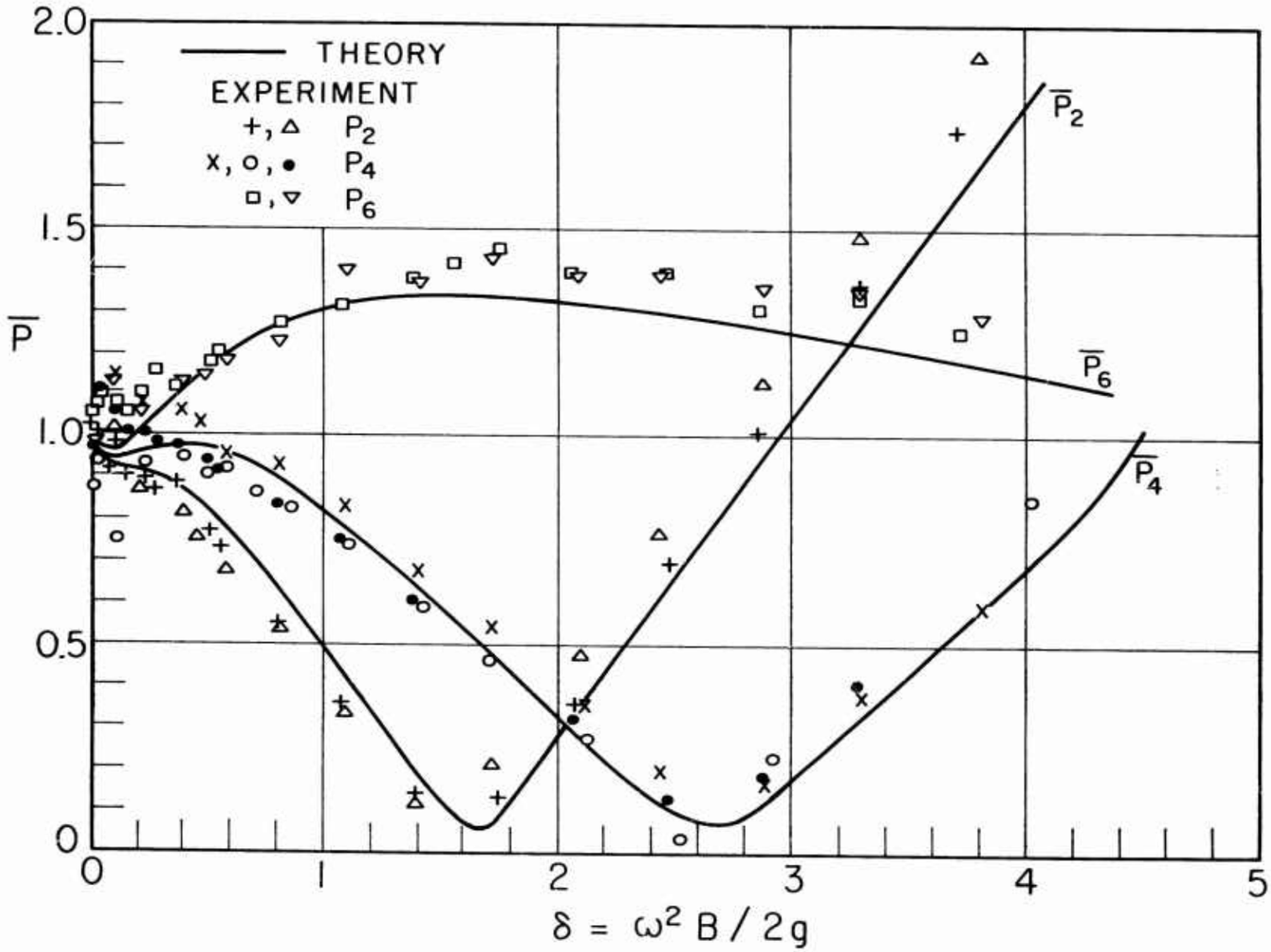

FIG. 15b $\overline{P}$ vs δ FOR MODEL 2

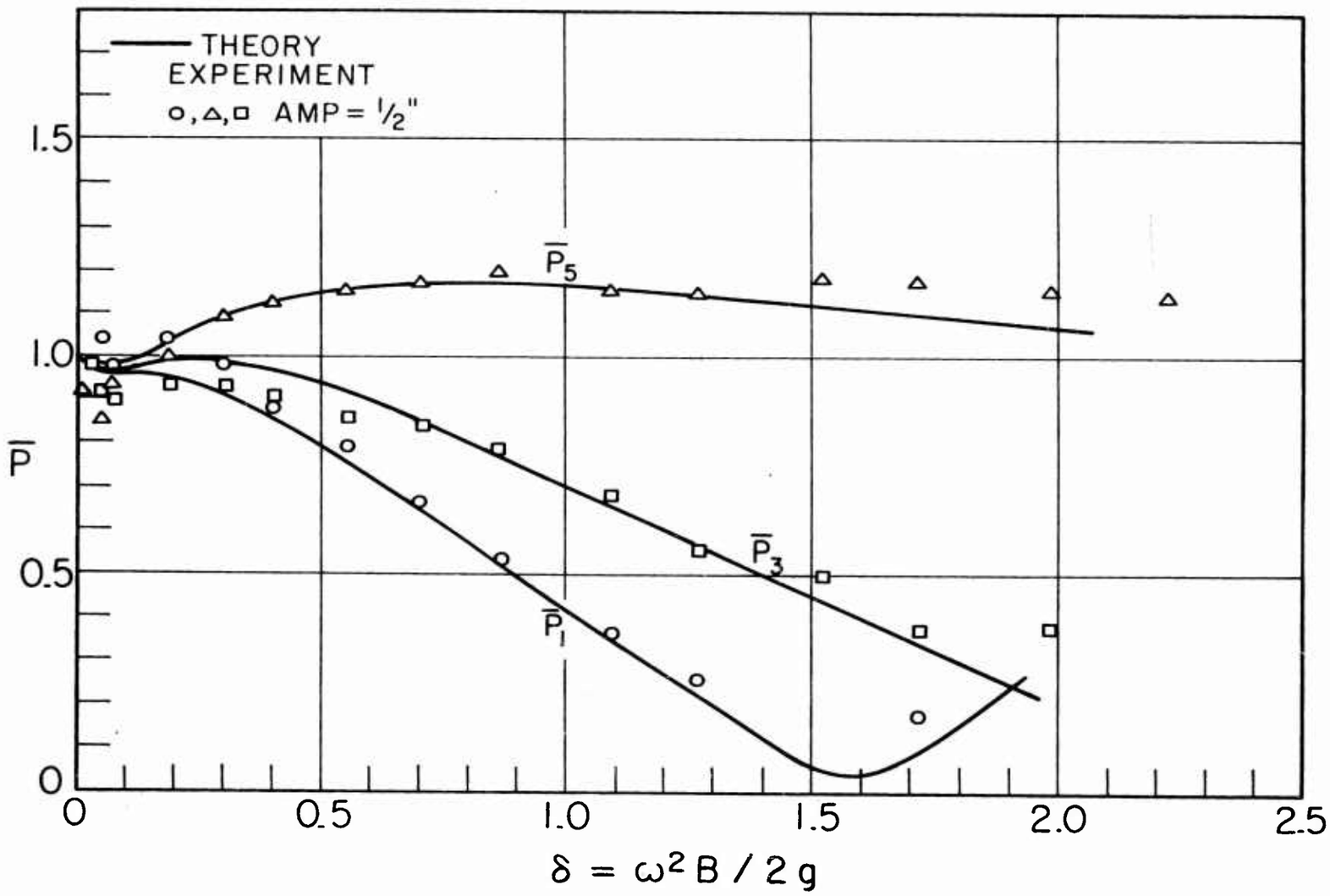

FIG. 16a $\overline{P}$ vs δ FOR MODEL 3

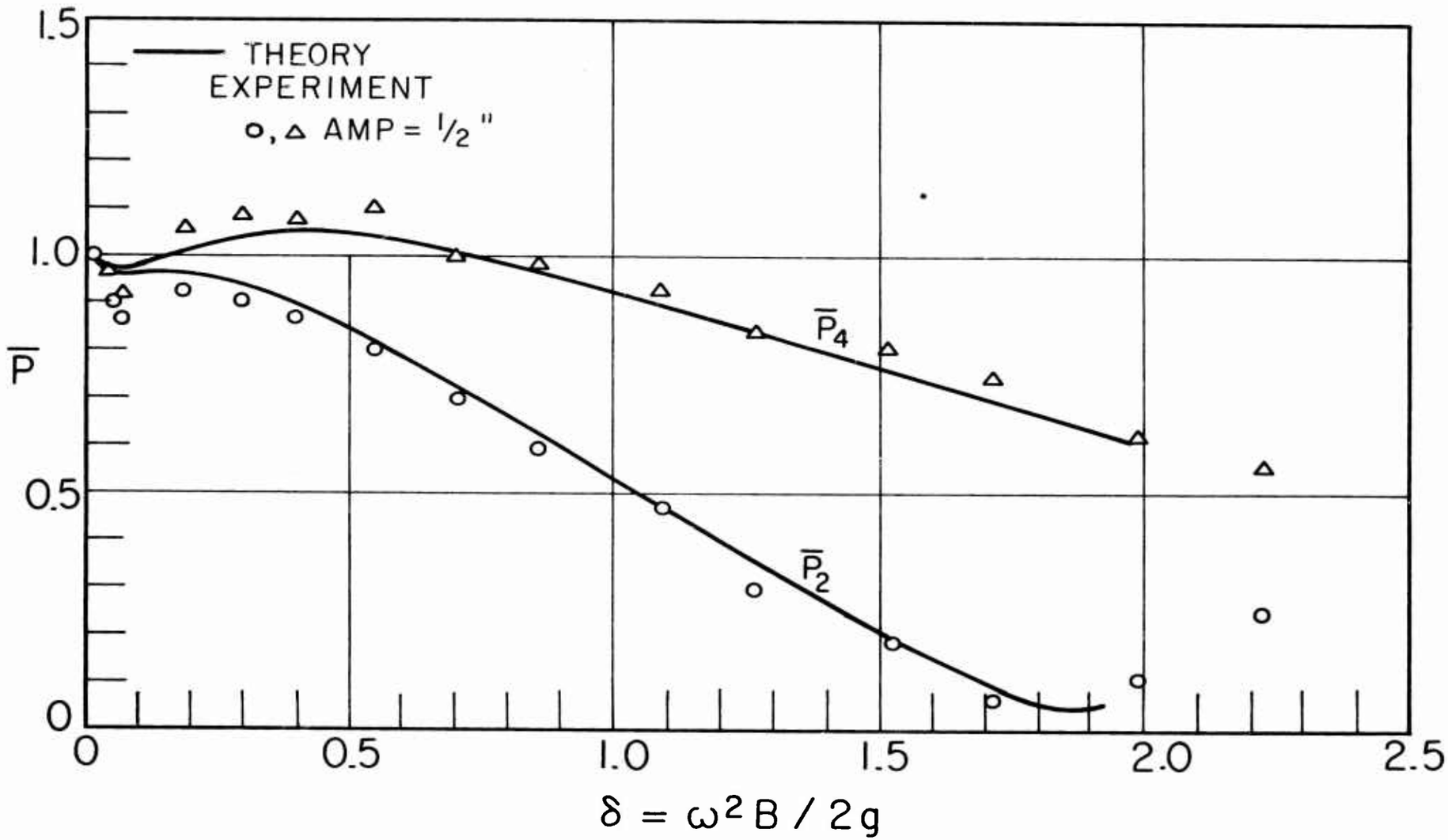

FIG. 16b $\overline{P}$ vs δ FOR MODEL 3

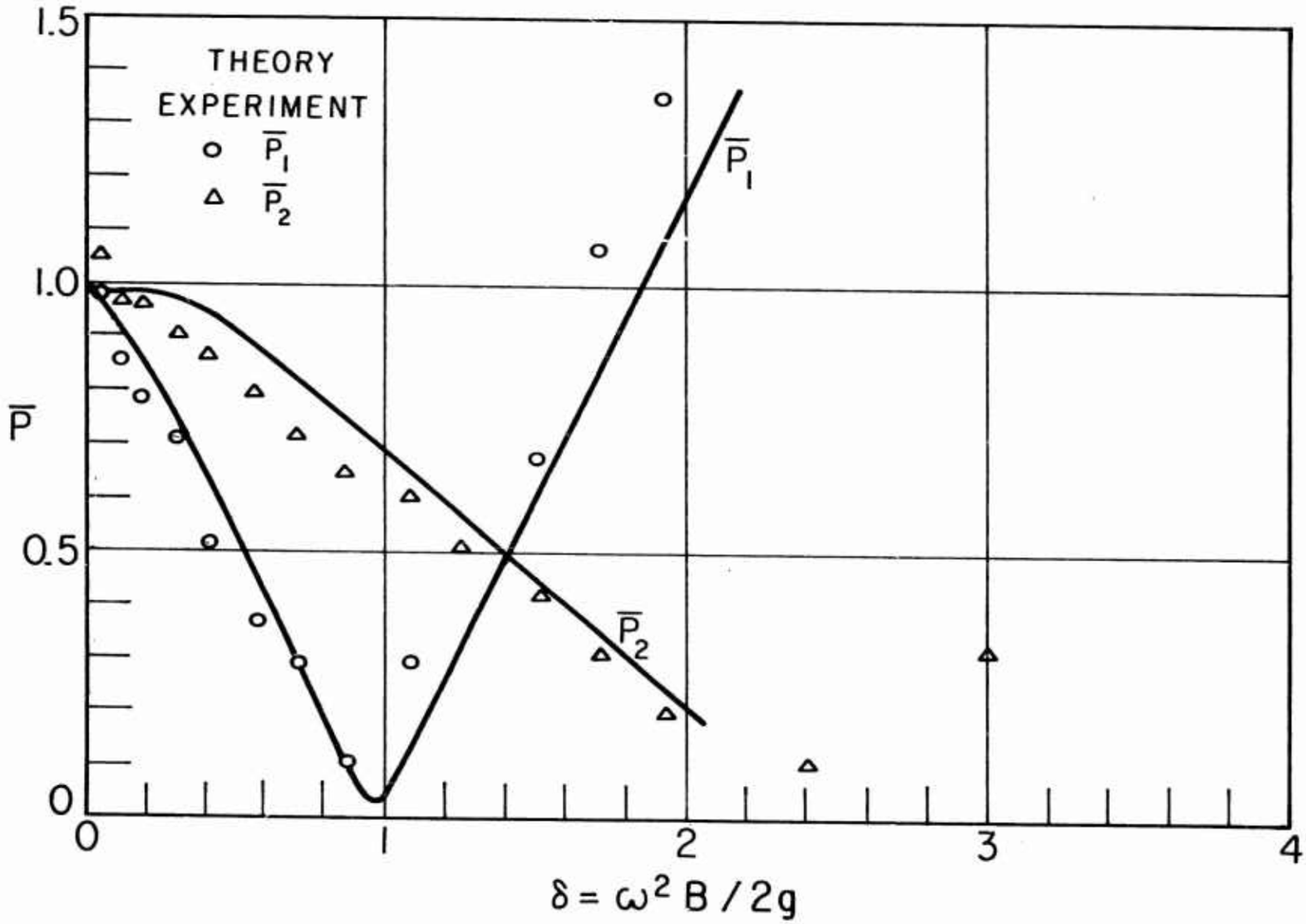

FIG. 17 a $\overline{P}$ vs δ FOR MODEL 4

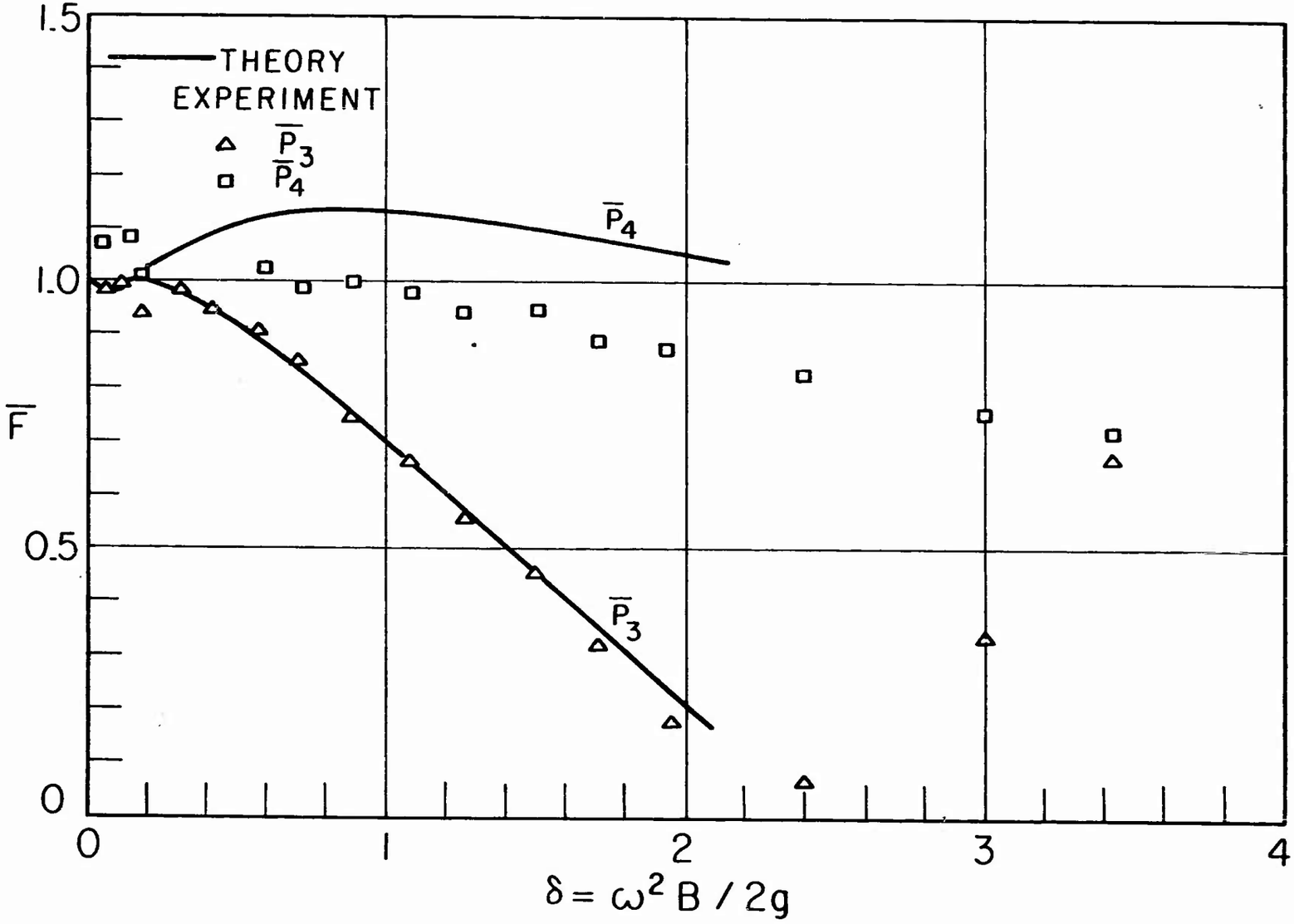

FIG. 17b $\overline{F}$ vs δ FOR MODEL 4

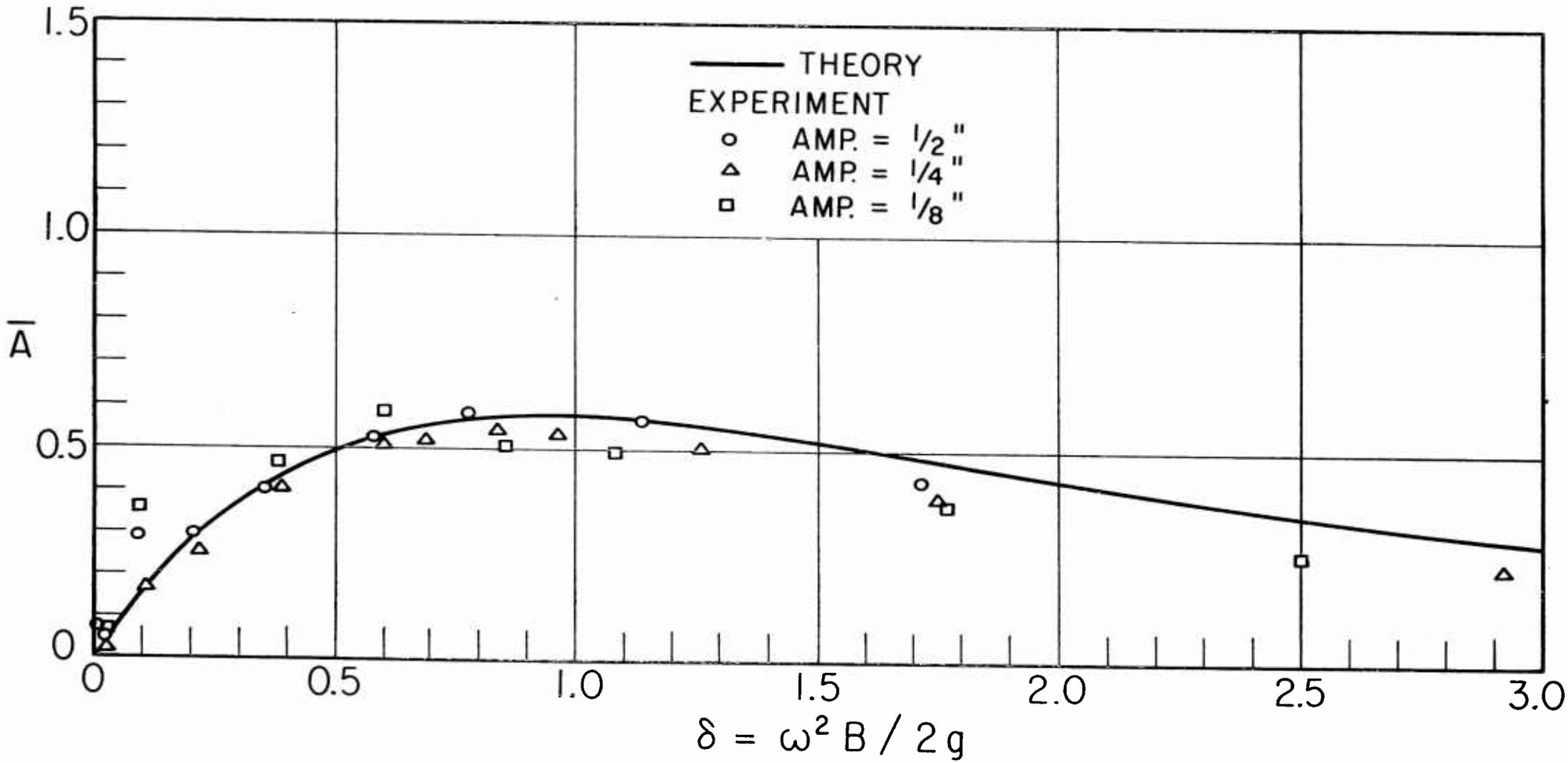

FIG. 18 $\overline{A}$ vs δ FOR MODEL 1

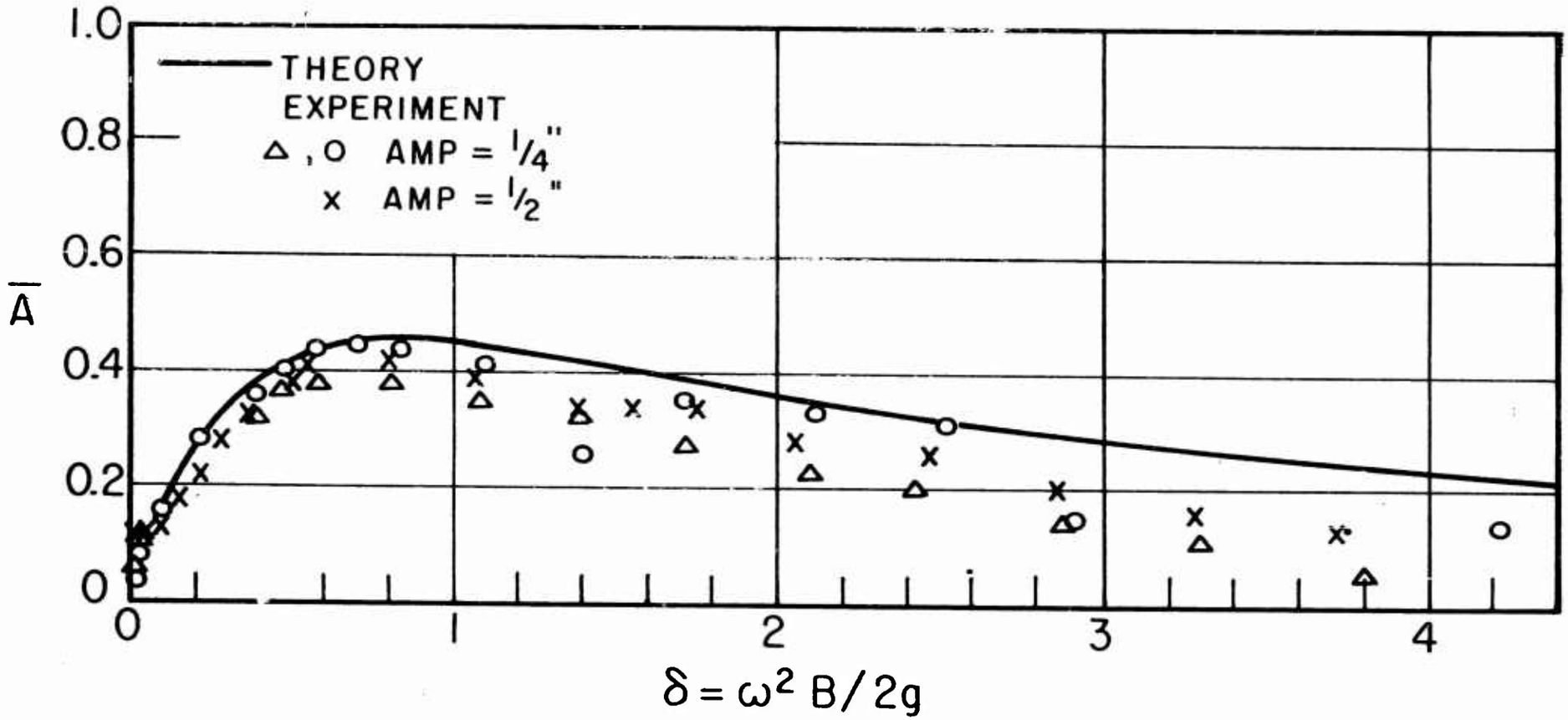

FIG. 19 $\overline{A}$ vs δ FOR MODEL 2

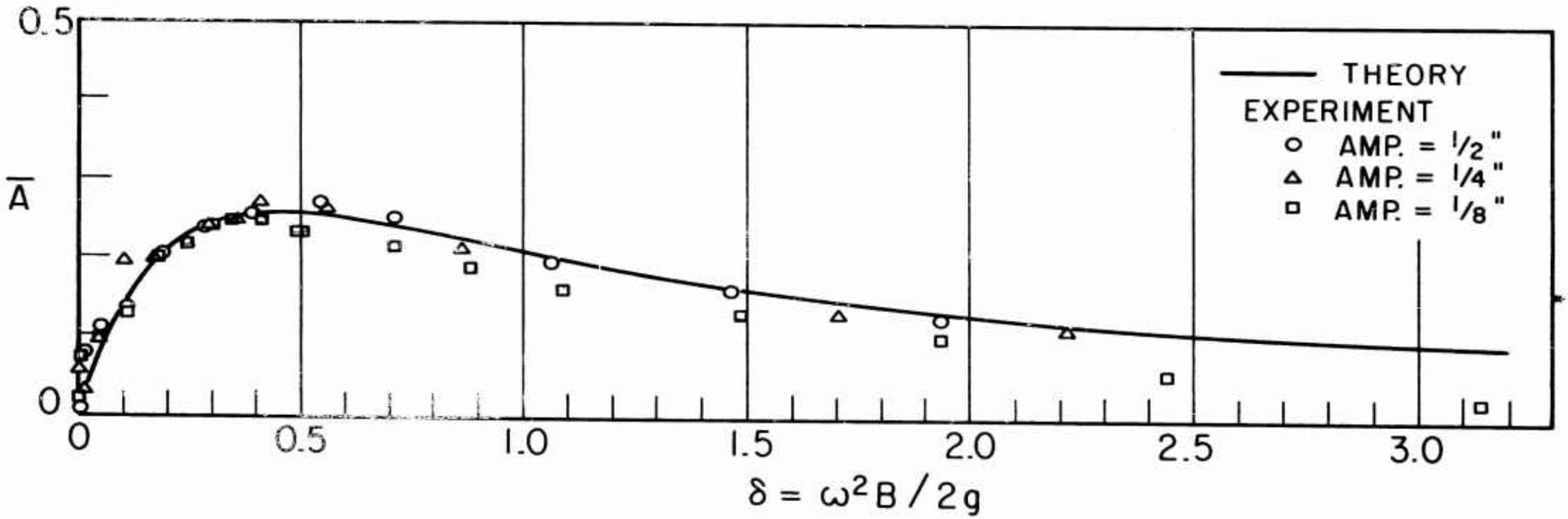

FIG. 20 $\overline{A}$ vs δ FOR MODEL 3

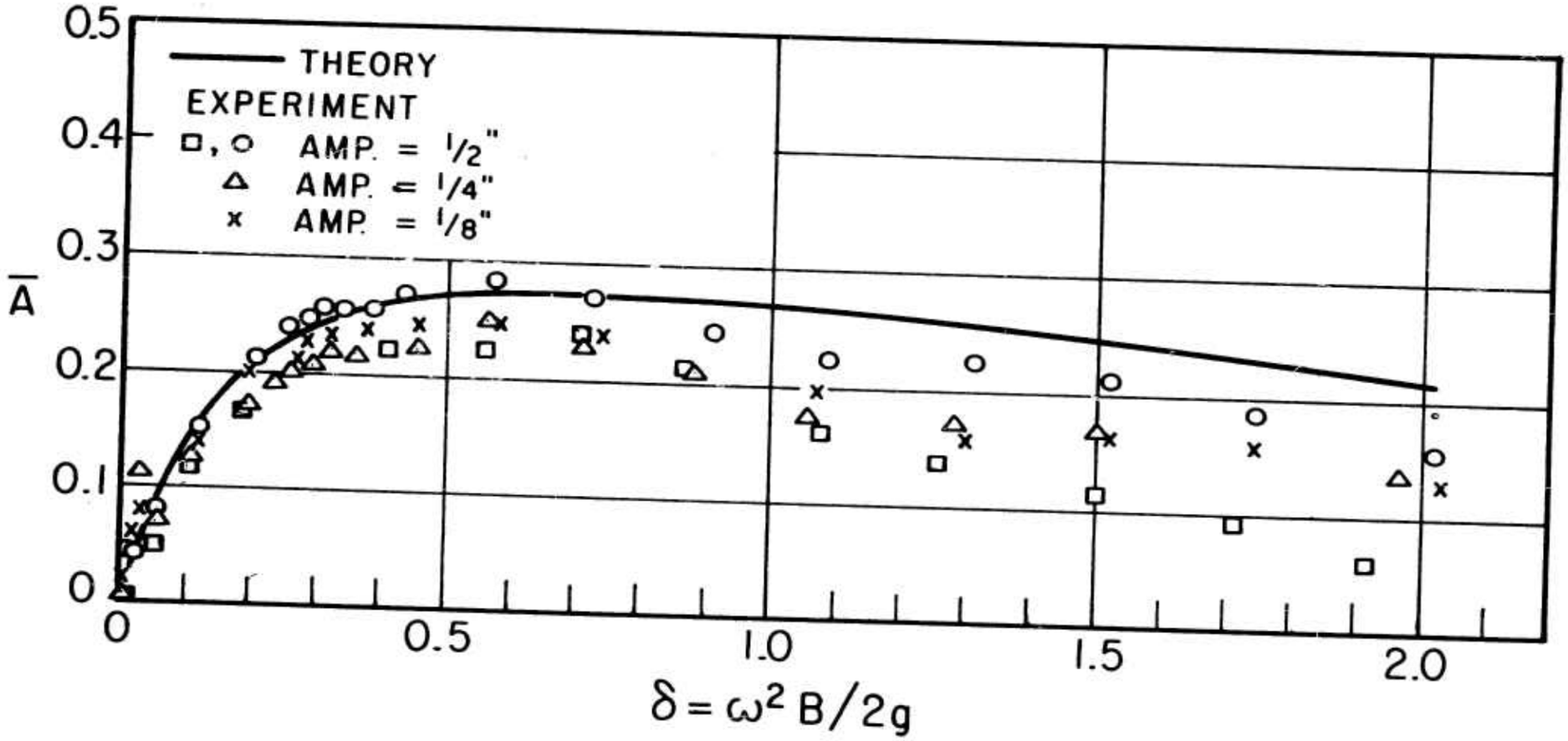

FIG. 21 $\overline{A}$ vs δ FOR MODEL 4

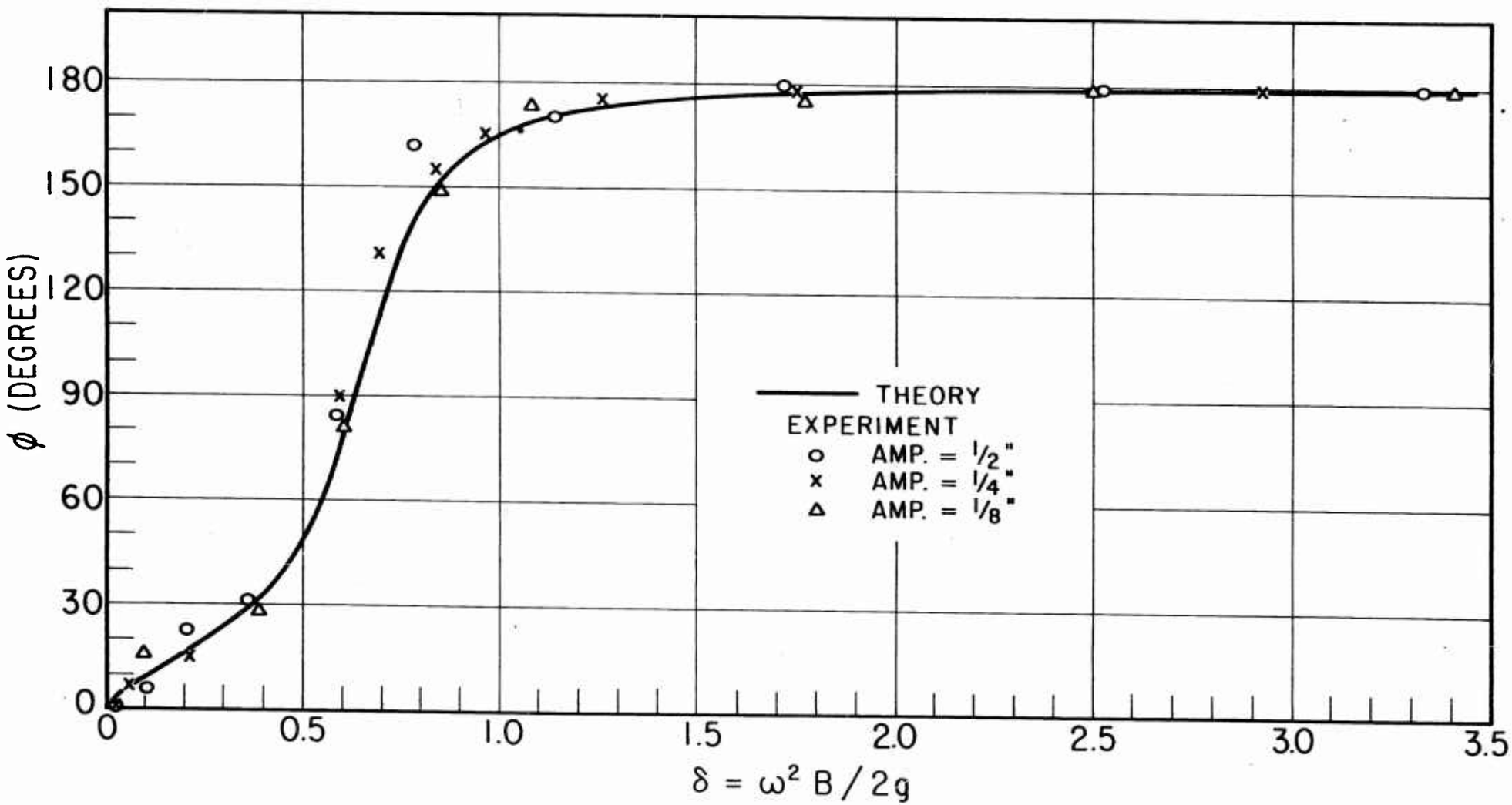

FIG. 22 FORCE PHASE ANGLE, ϕ, vs δ FOR MODEL 1

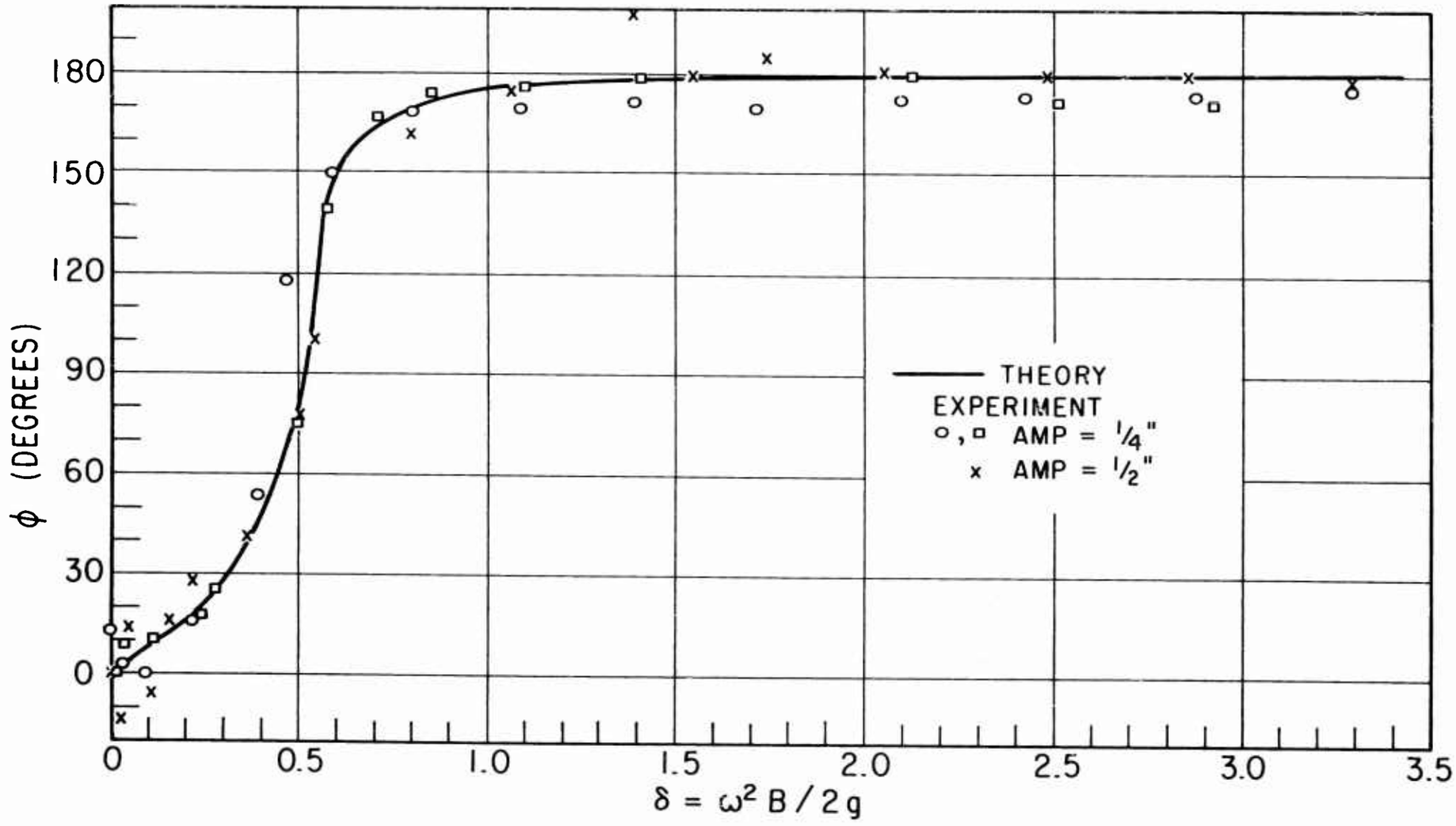

FIG. 23 FORCE PHASE ANGLE, ϕ, vs δ FOR MODEL 2

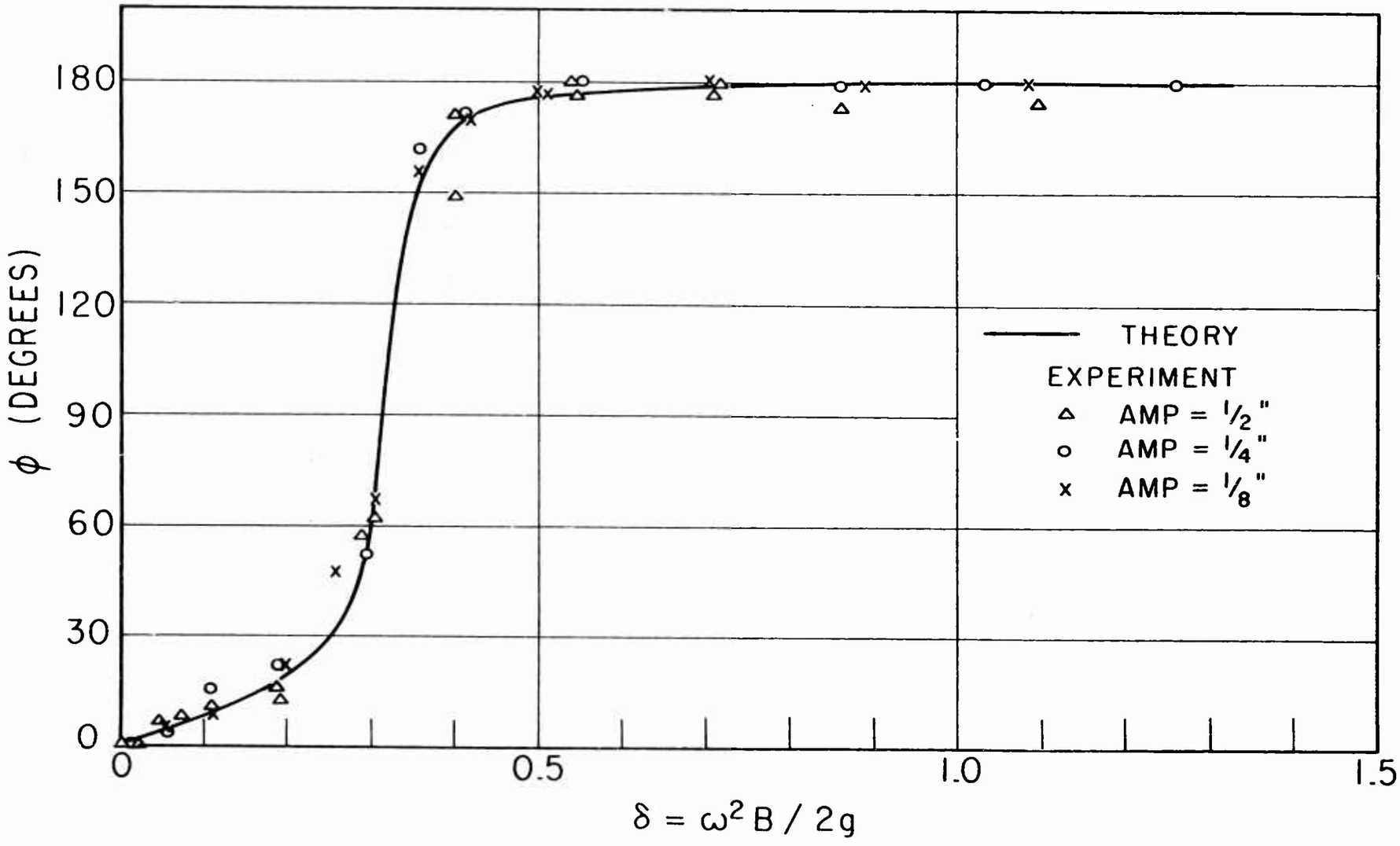

FIG. 24 FORCE PHASE ANGLE, ϕ, vs δ FOR MODEL 3

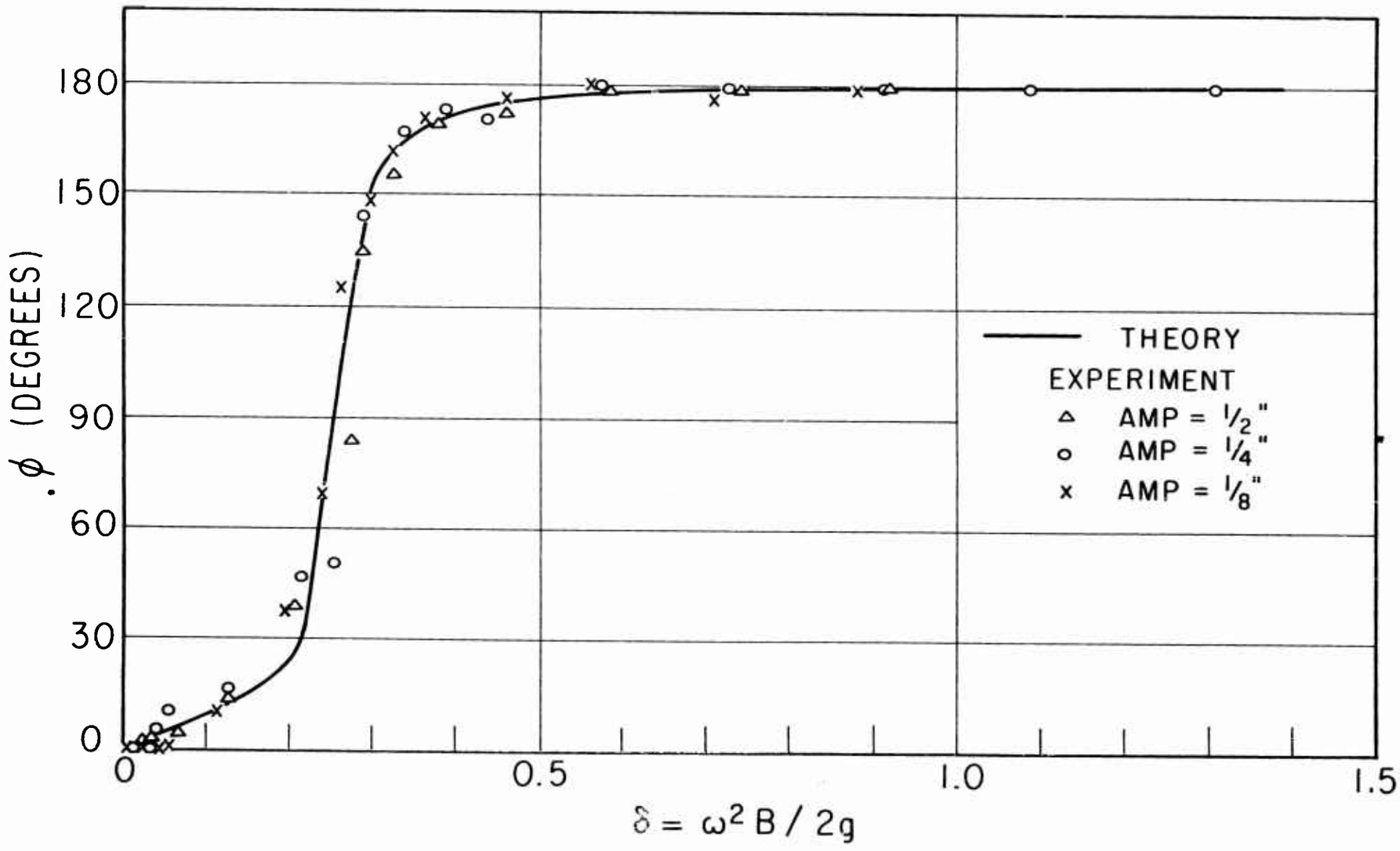

FIG. 25 FORCE PHASE ANGLE, ϕ, vs δ FOR MODEL 4

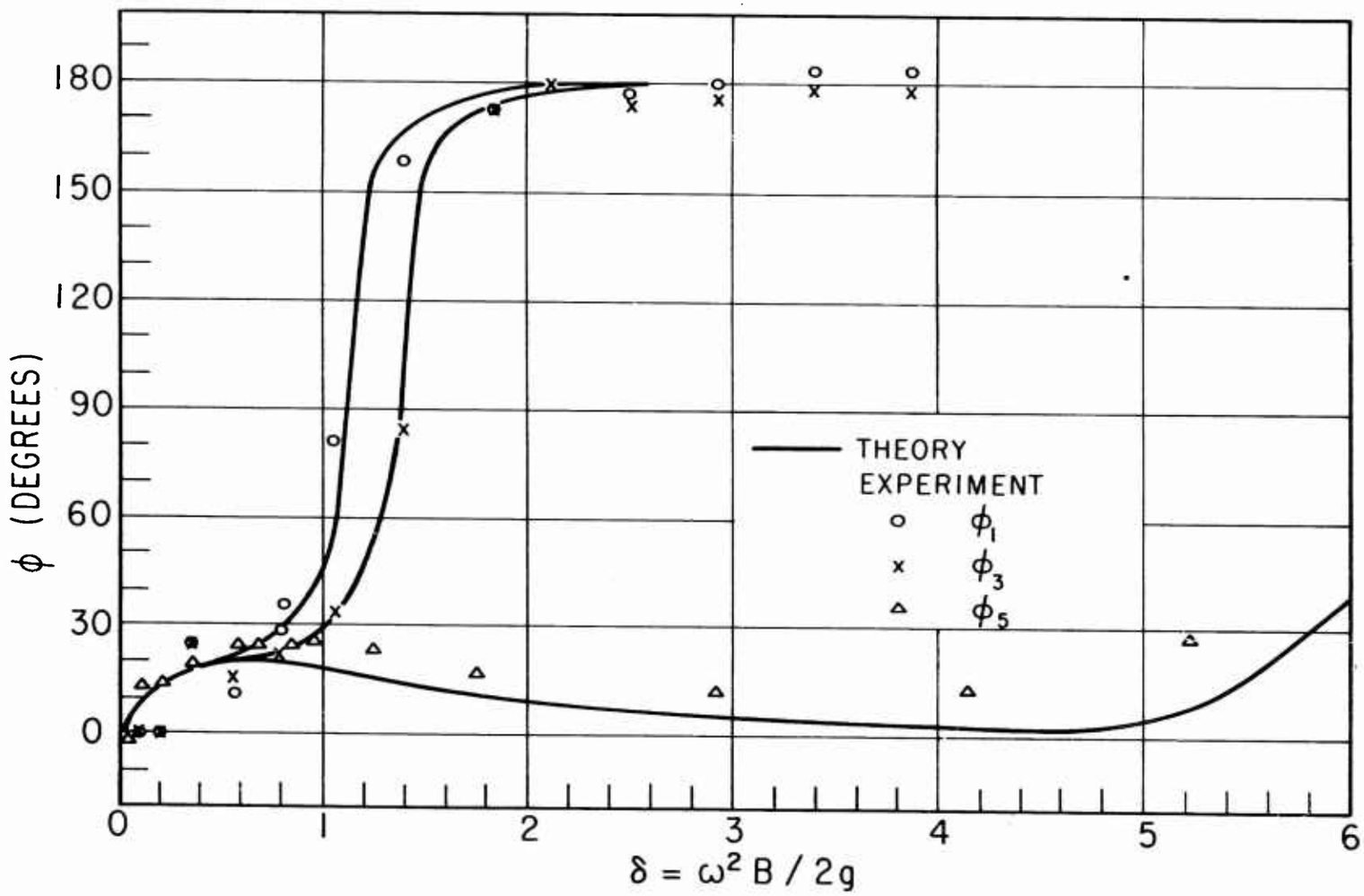

FIG. 26a PRESSURE PHASE ANGLE, ϕ, vs δ FOR MODEL 1

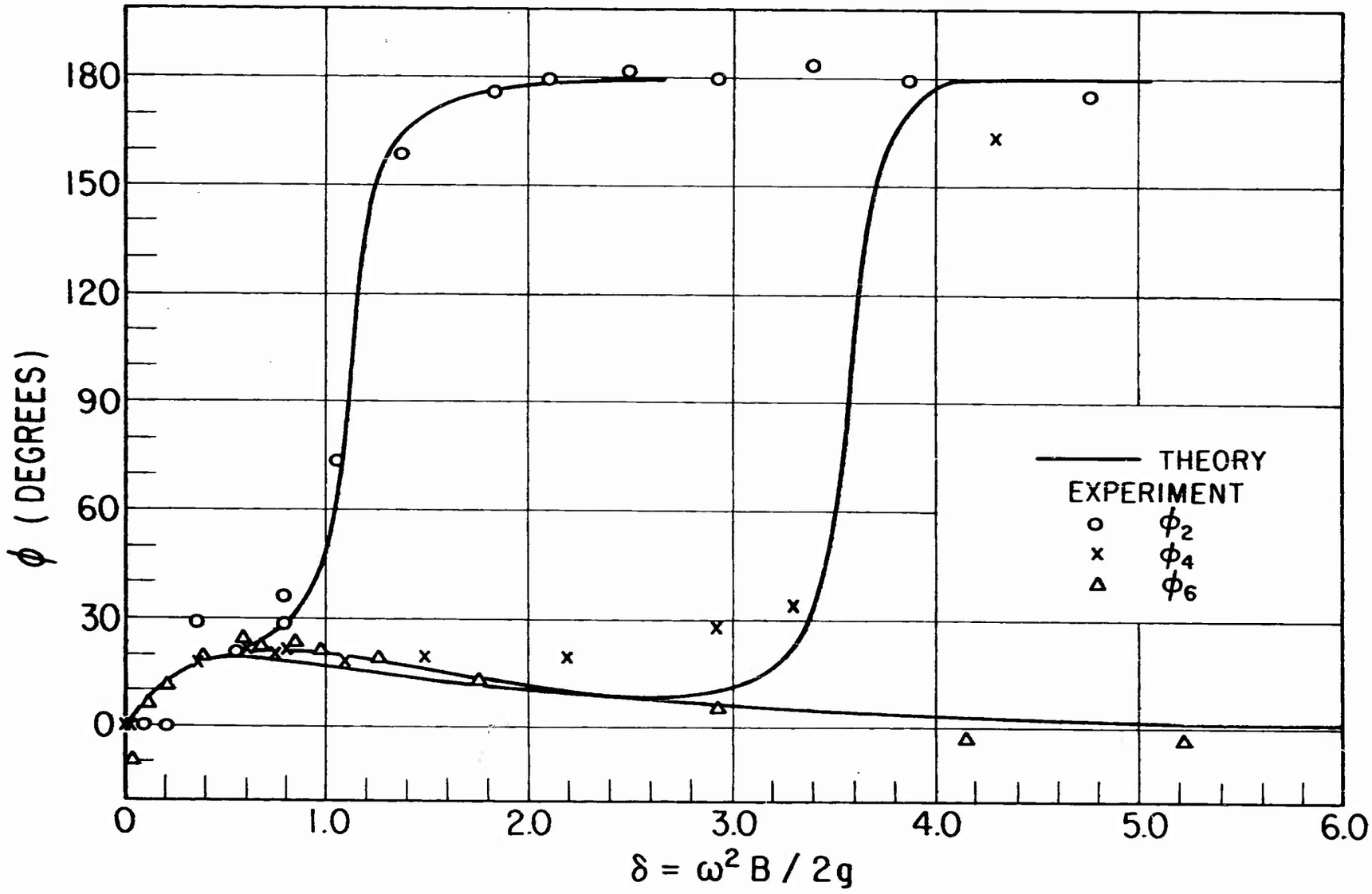

FIG. 26b PRESSURE PHASE ANGLE, ϕ, vs δ FOR MODEL 1

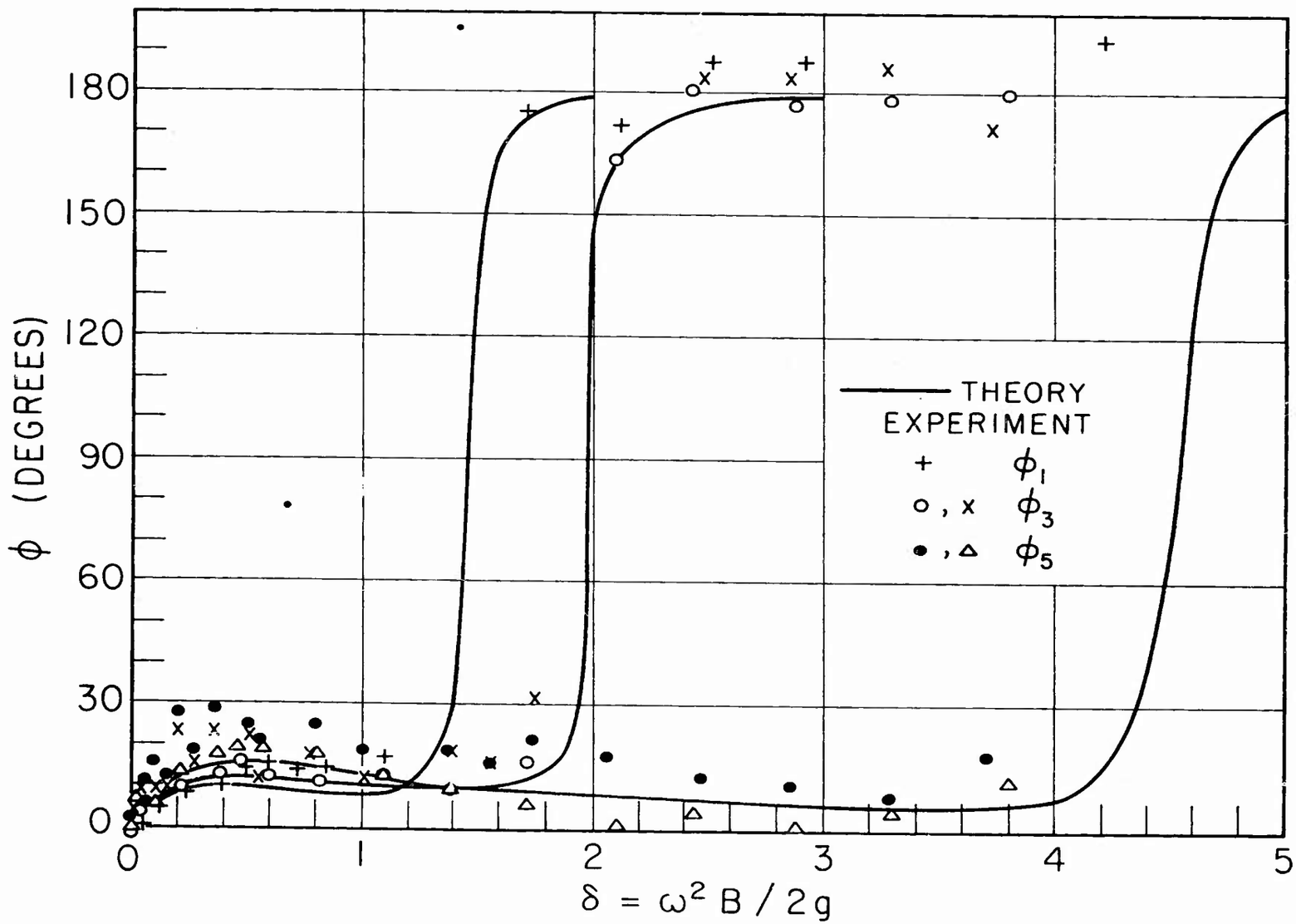

FIG. 27a PRESSURE PHASE ANGLE, ϕ, vs δ FOR MODEL 2

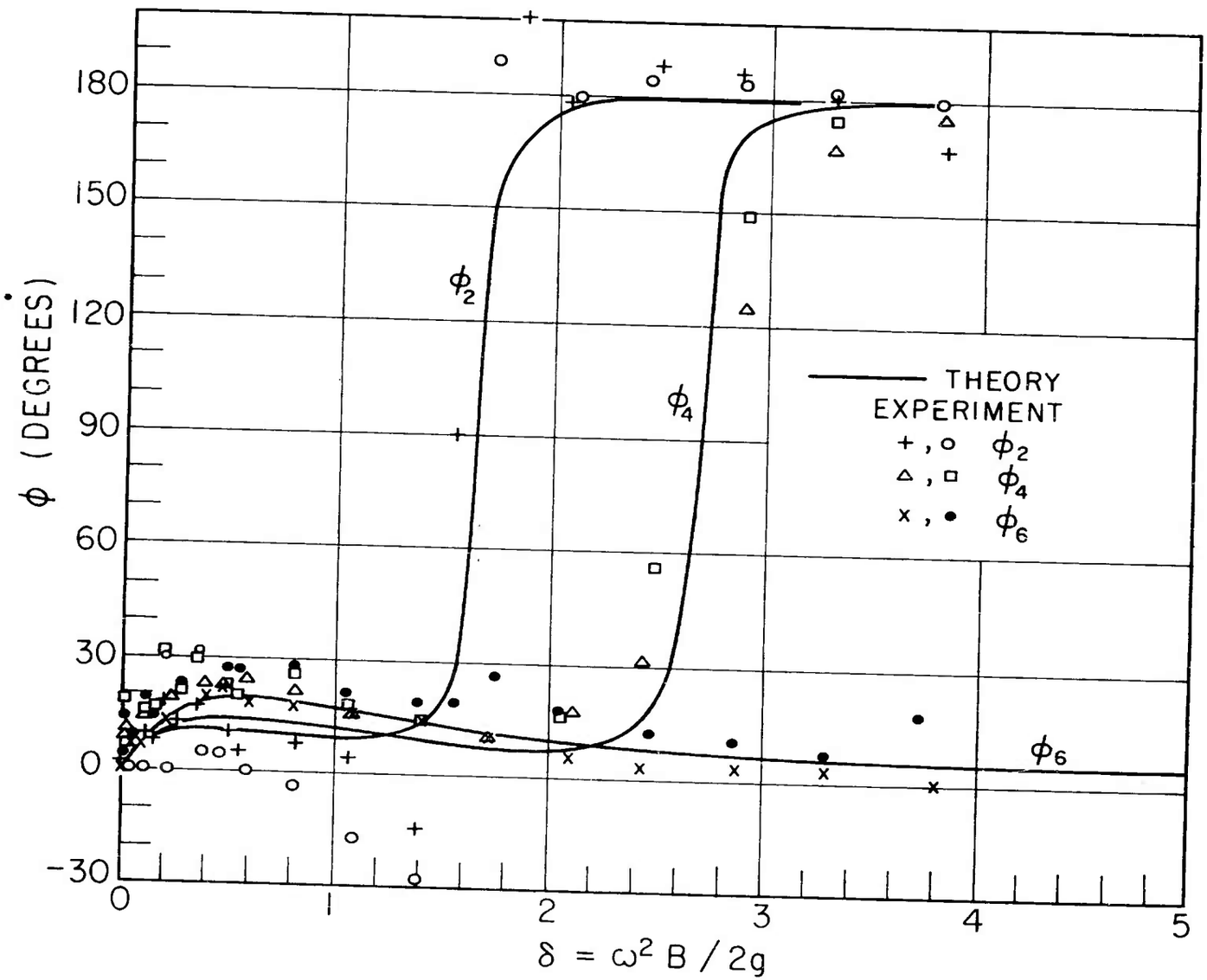

FIG. 27b PRESSURE PHASE ANGLE, ϕ, vs δ FOR MODEL 2

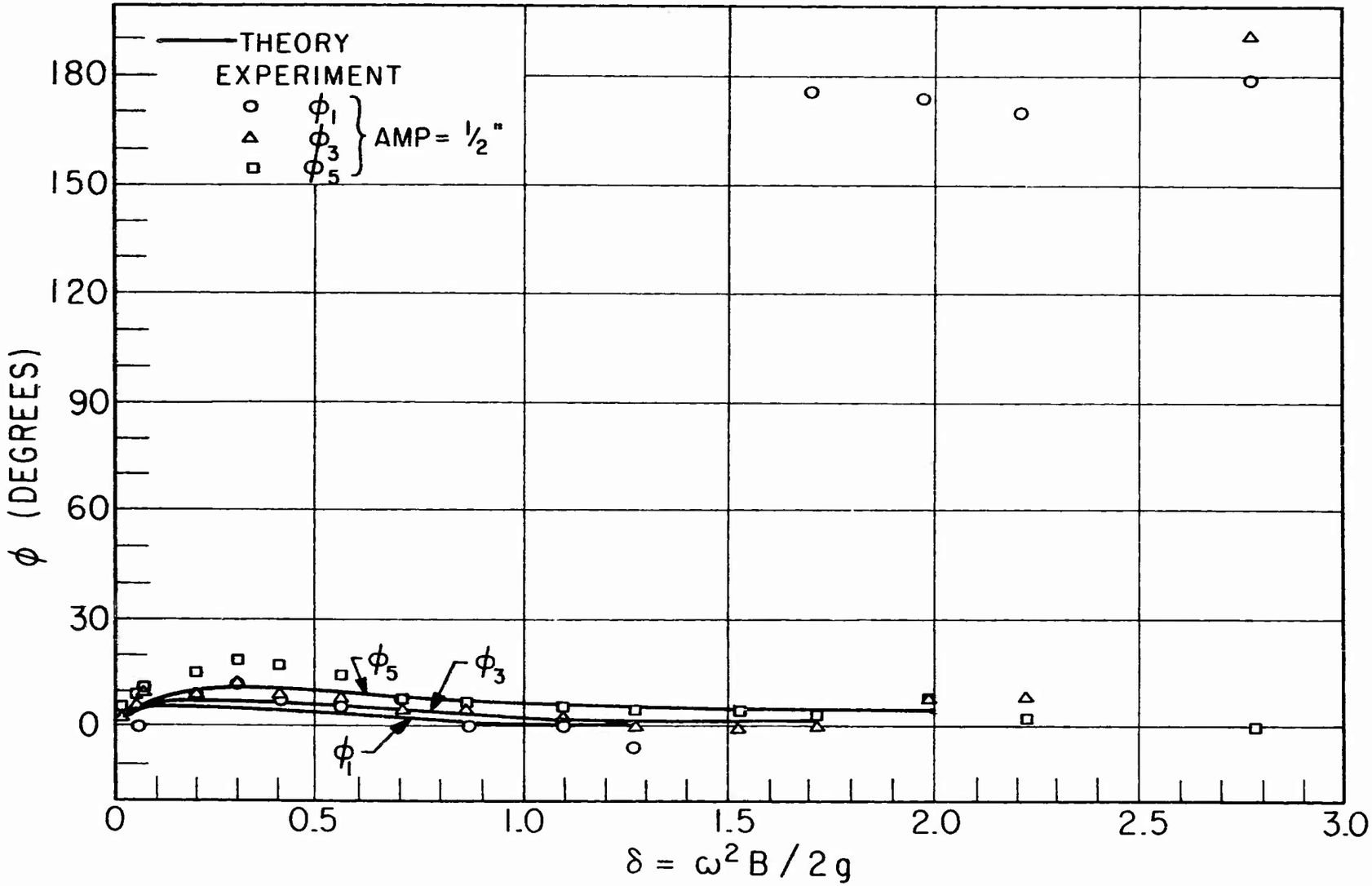

FIG. 28a PRESSURE PHASE ANGLE, ϕ, vs δ FOR MODEL 3

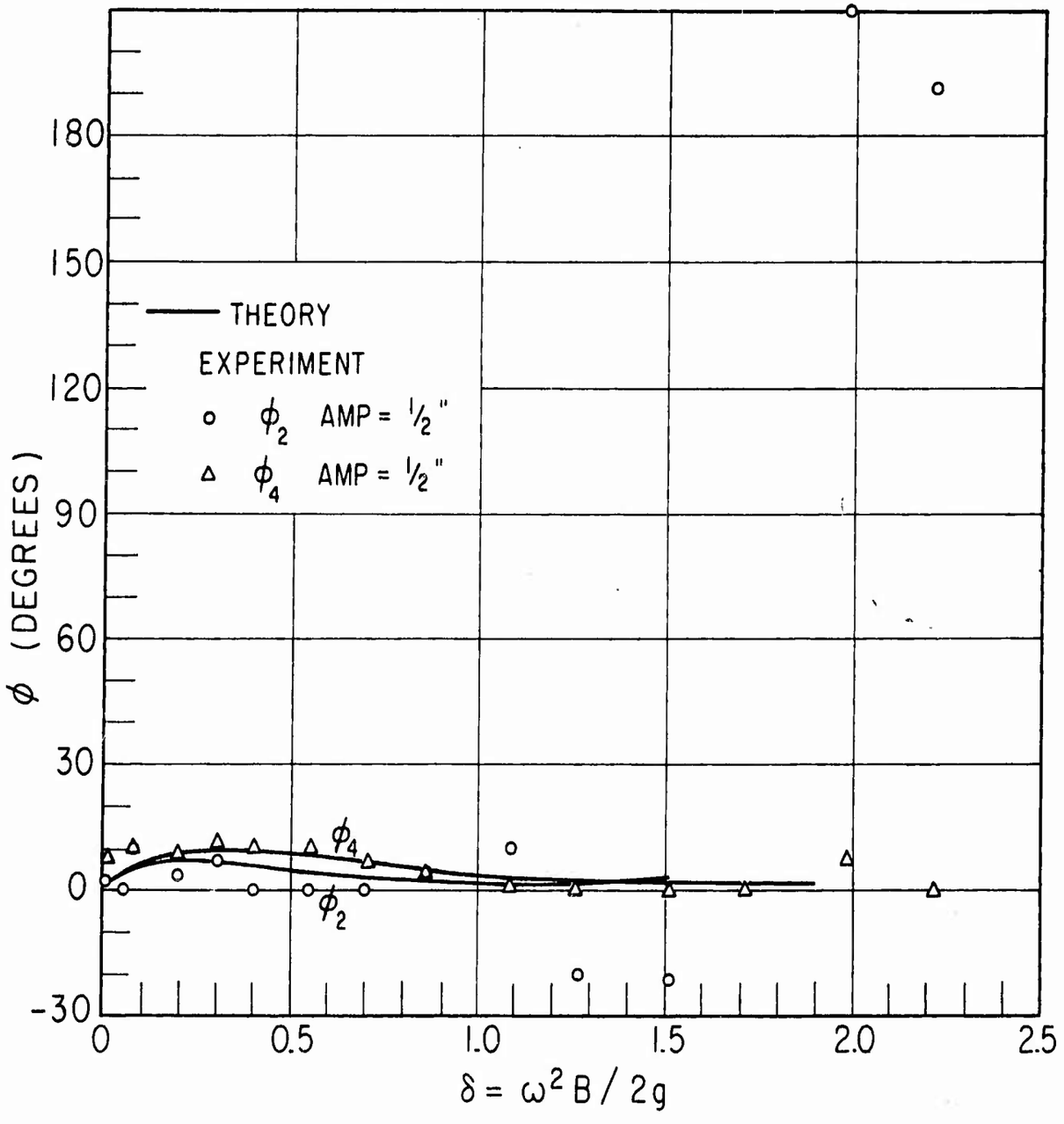

FIG. 28b PRESSURE PHASE ANGLE, ϕ, vs δ FOR MODEL 3

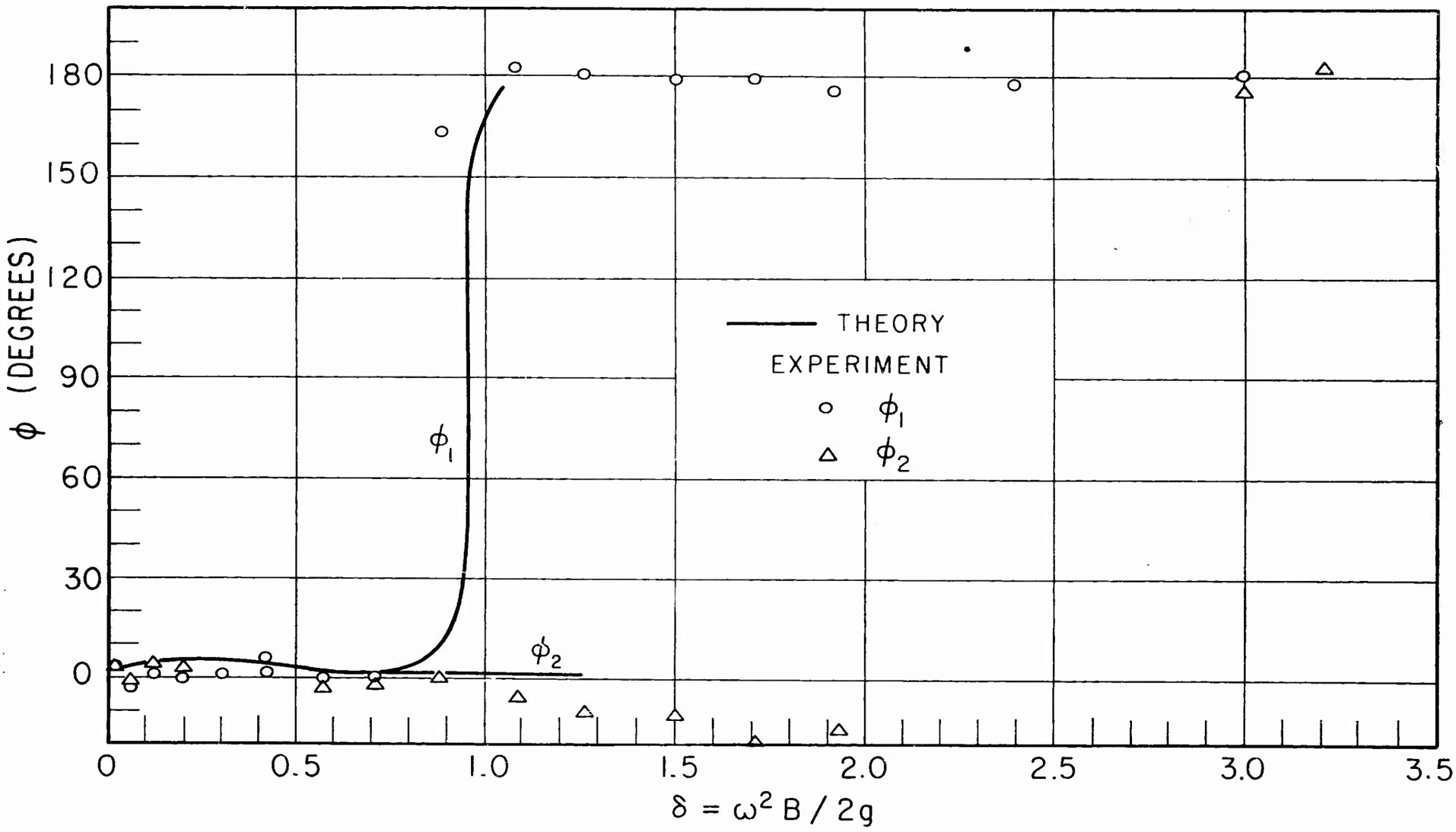

FIG. 29a PRESSURE PHASE ANGLE, ϕ, vs δ FOR MODEL 4

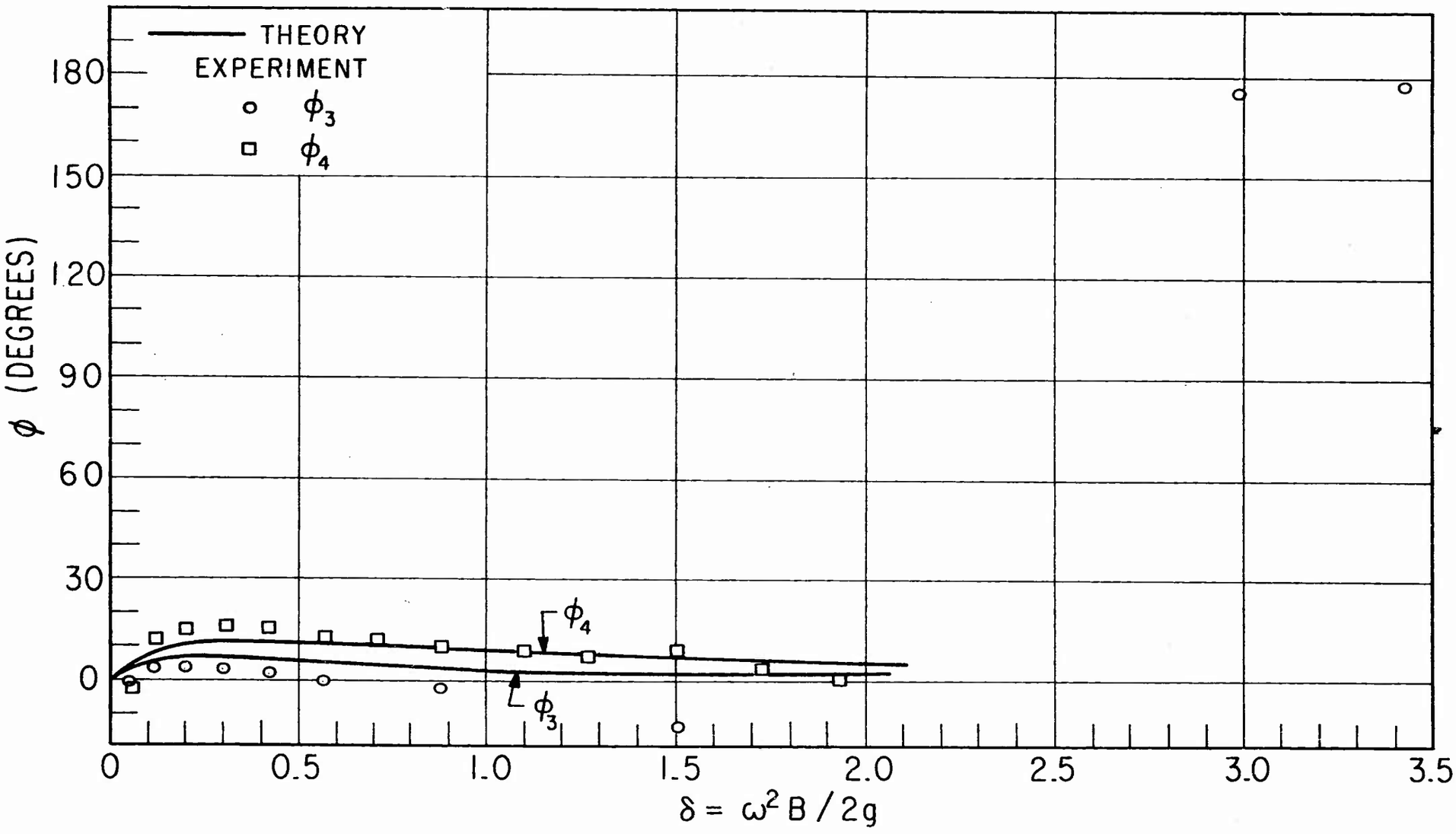

FIG. 29b PRESSURE PHASE ANGLE, ϕ, vs δ FOR MODEL 4

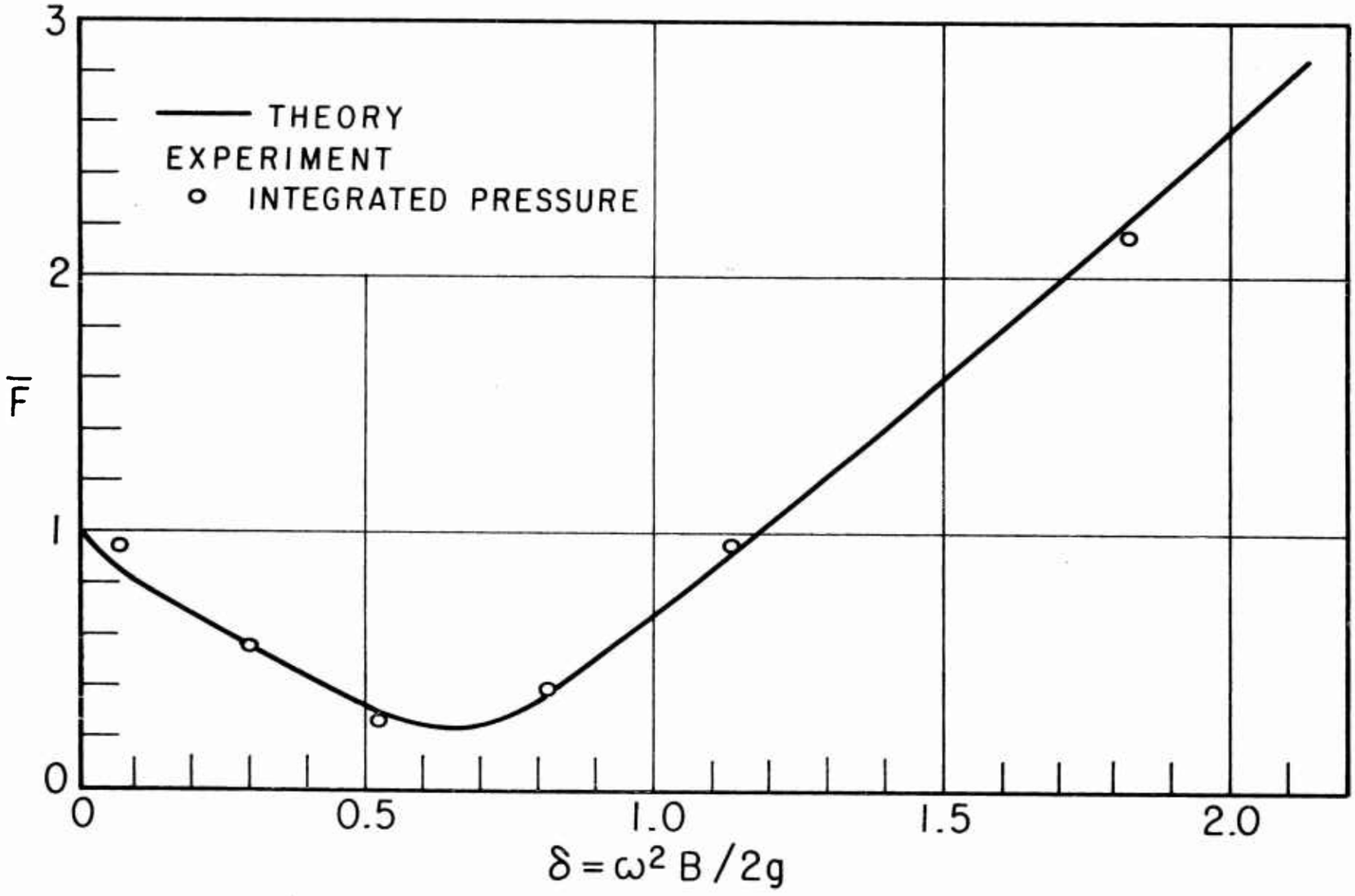

FIG. 30 $\overline{F}$ vs δ FOR MODEL 1

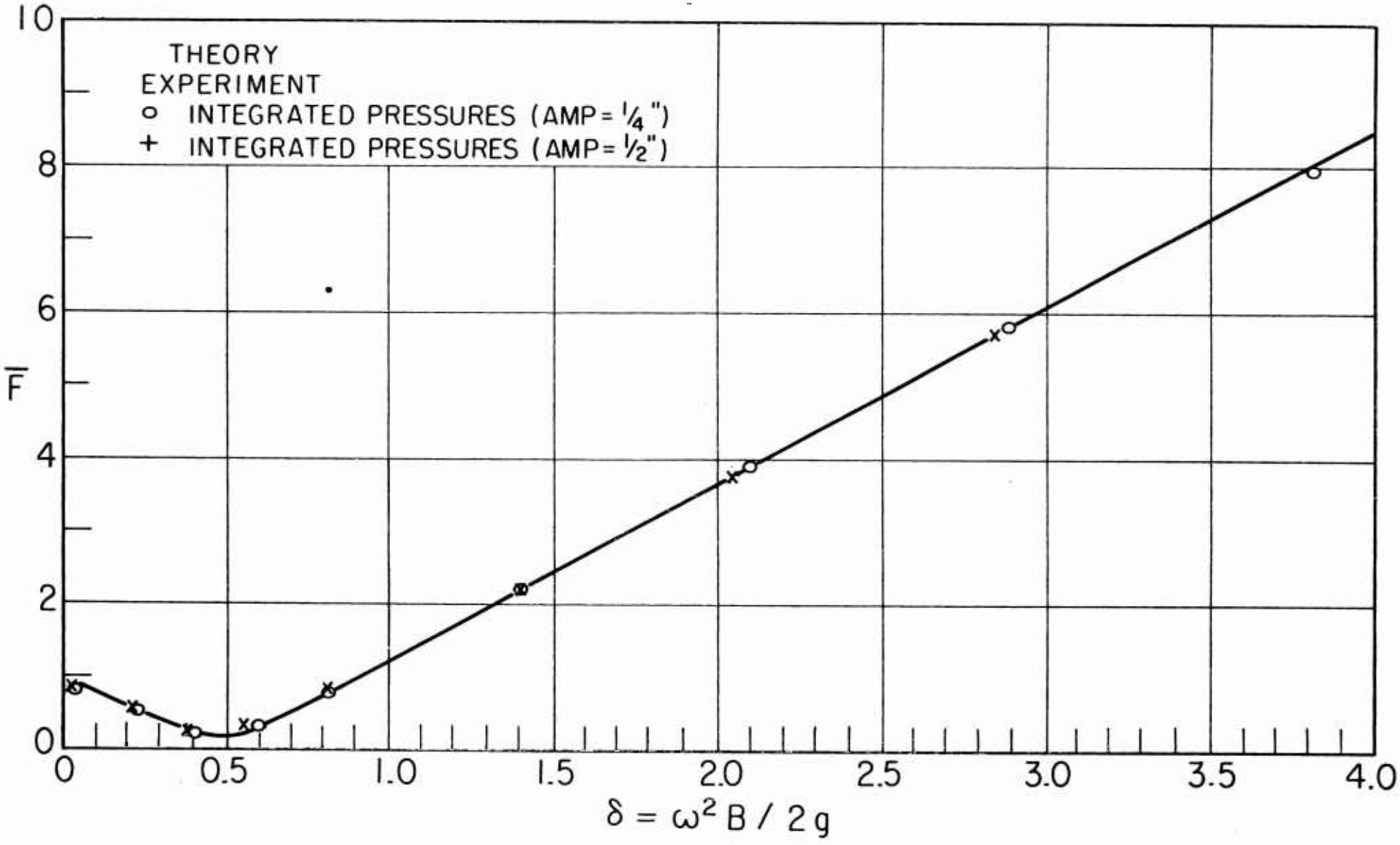

FIG. 31 $\overline{F}$ vs δ FOR MODEL 2

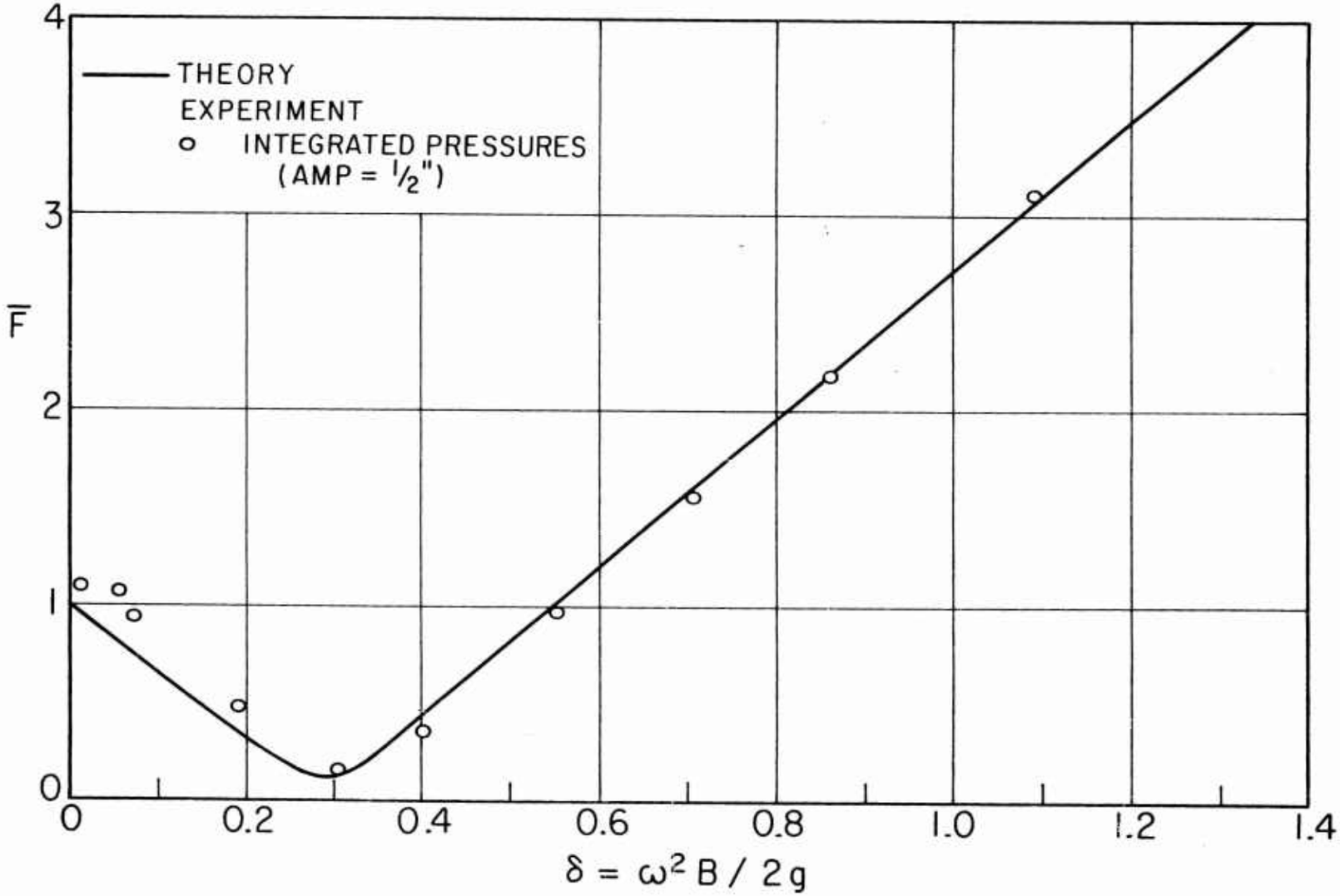

FIG. 32 $\overline{F}$ vs δ FOR MODEL 3

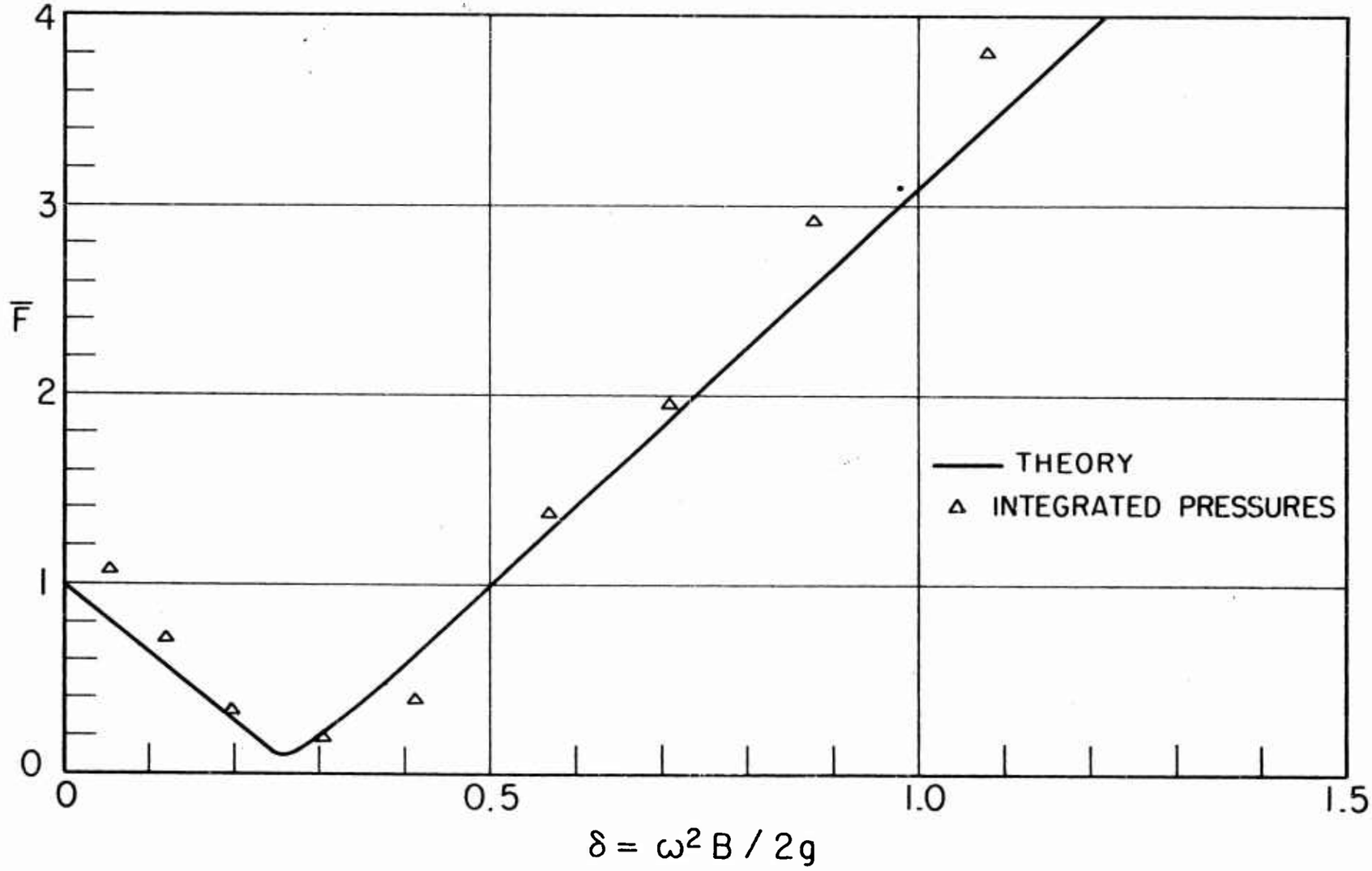

FIG. 33 $\overline{F}$ vs δ FOR MODEL 4

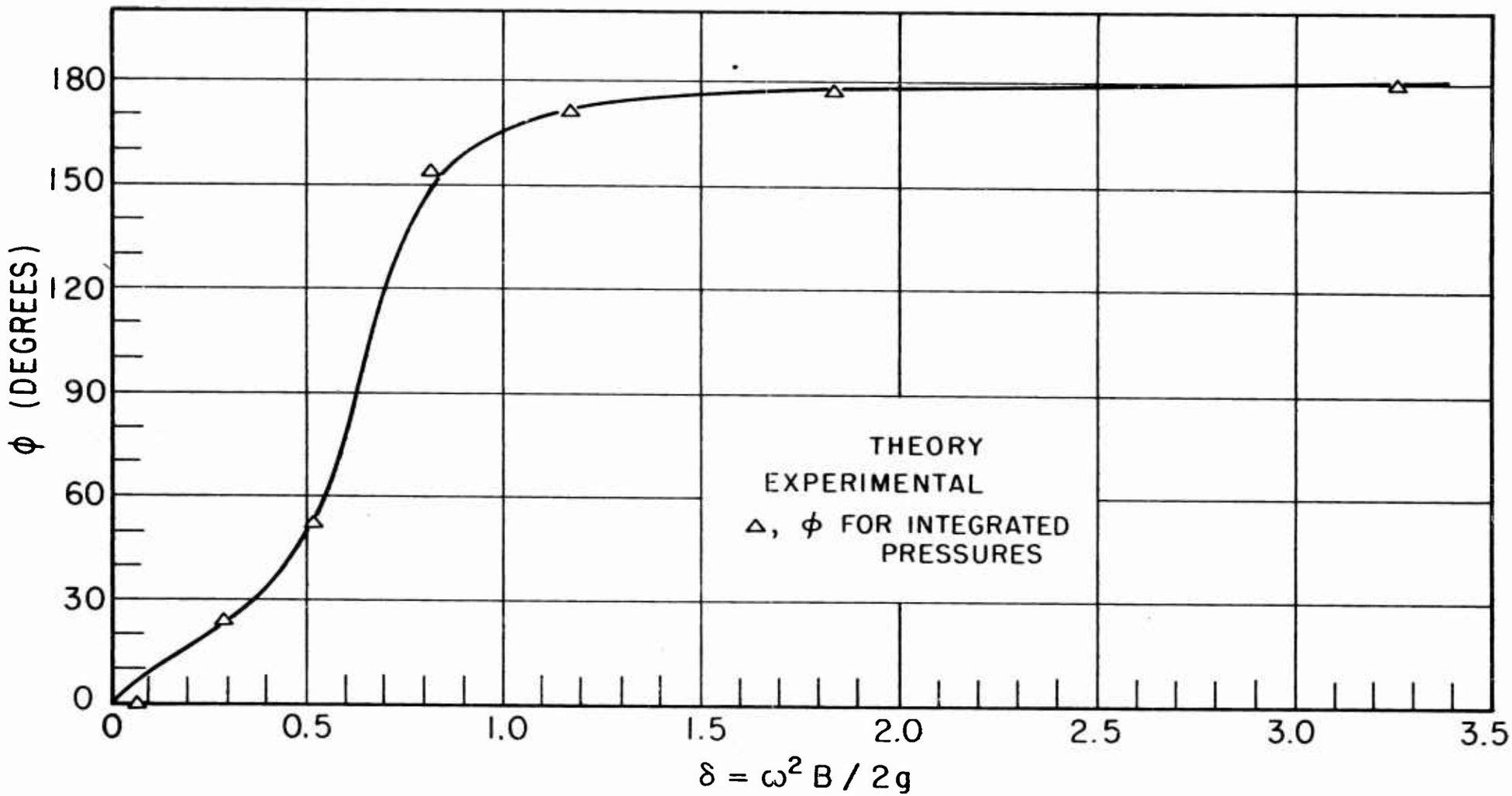

FIG. 34 FORCE PHASE ANGLE, ϕ, vs δ FOR MODEL 1

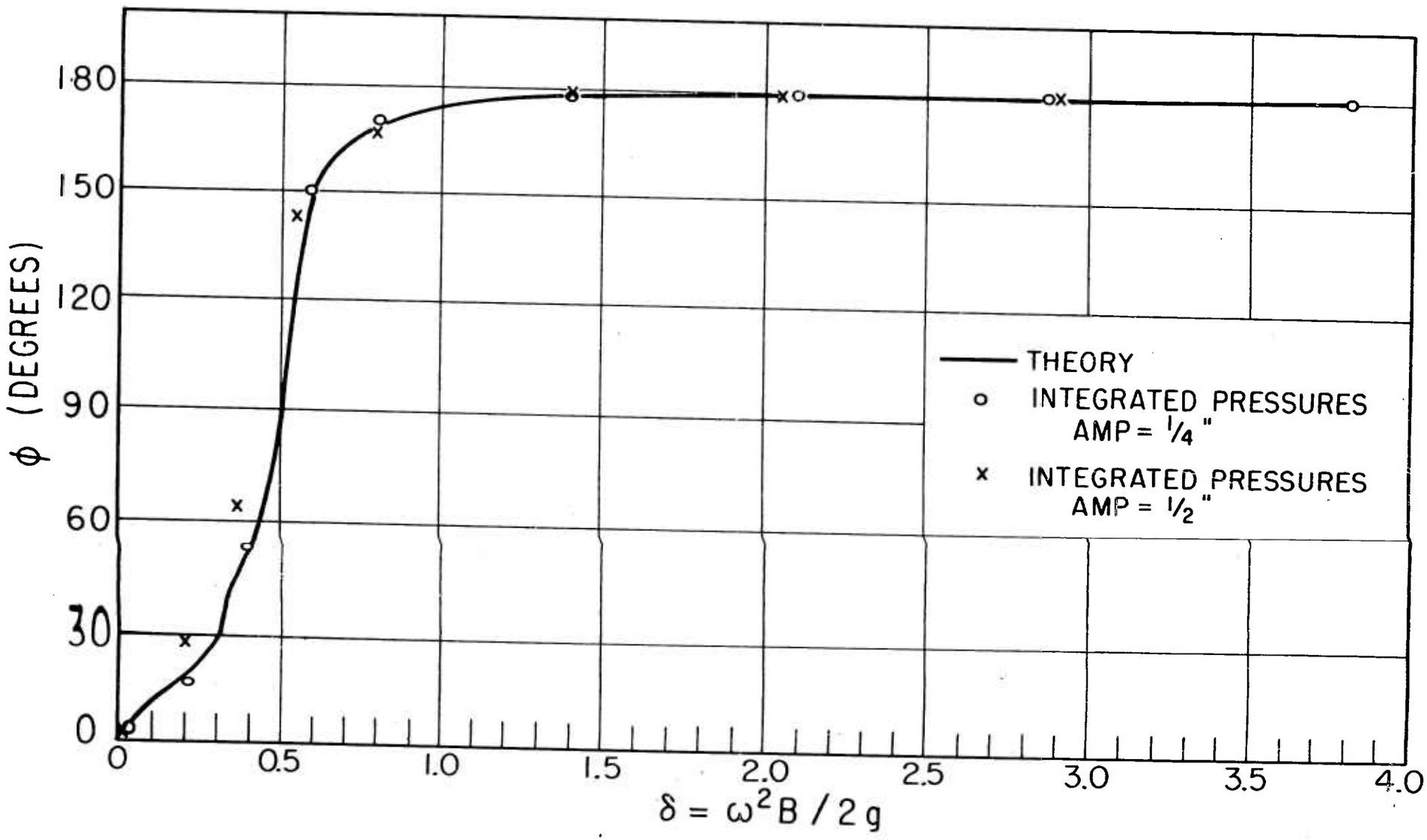

FIG. 35 FORCE PHASE ANGLE, ϕ, vs δ FOR MODEL 2

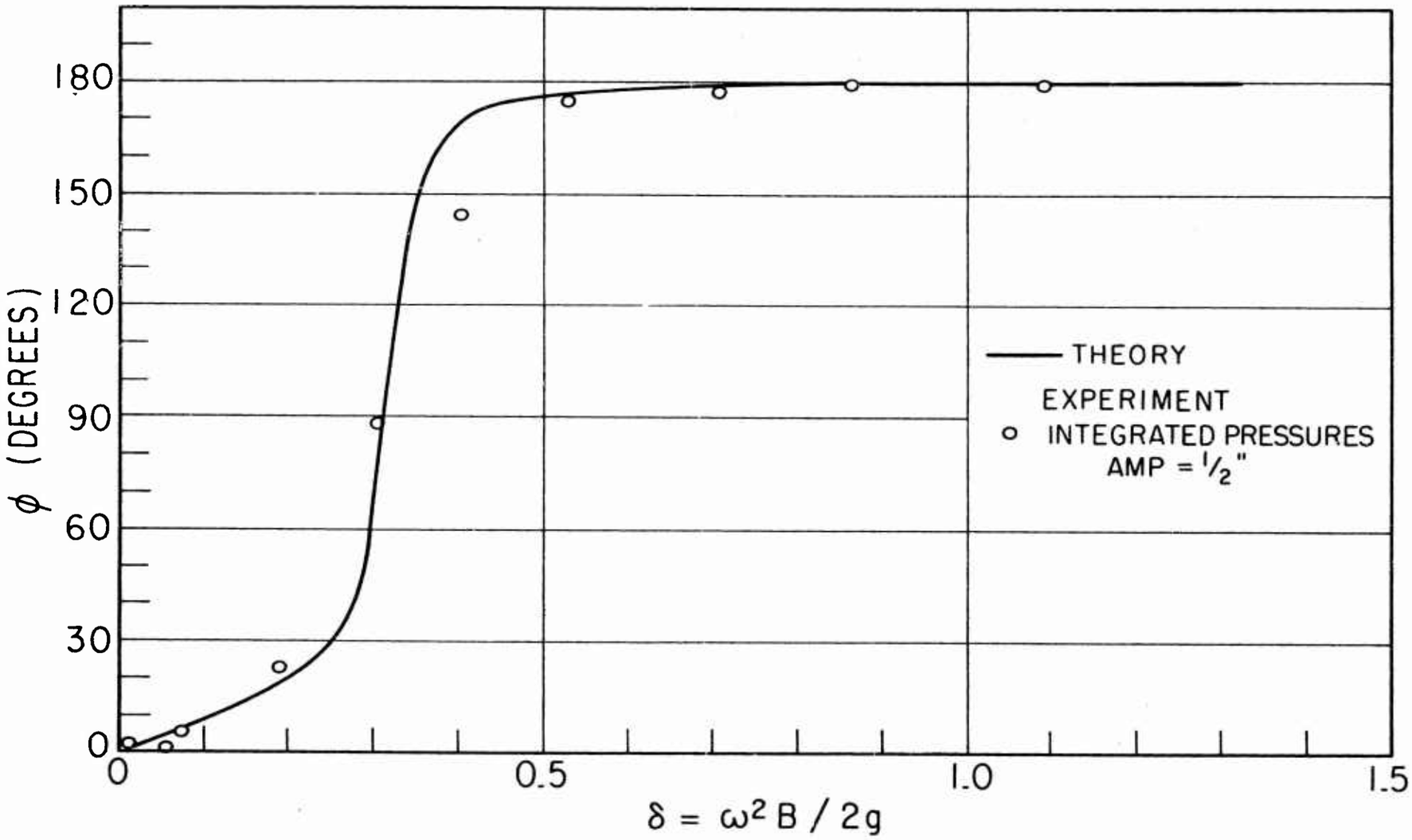

FIG. 36 FORCE PHASE ANGLE ϕ , vs δ FOR MODEL 3

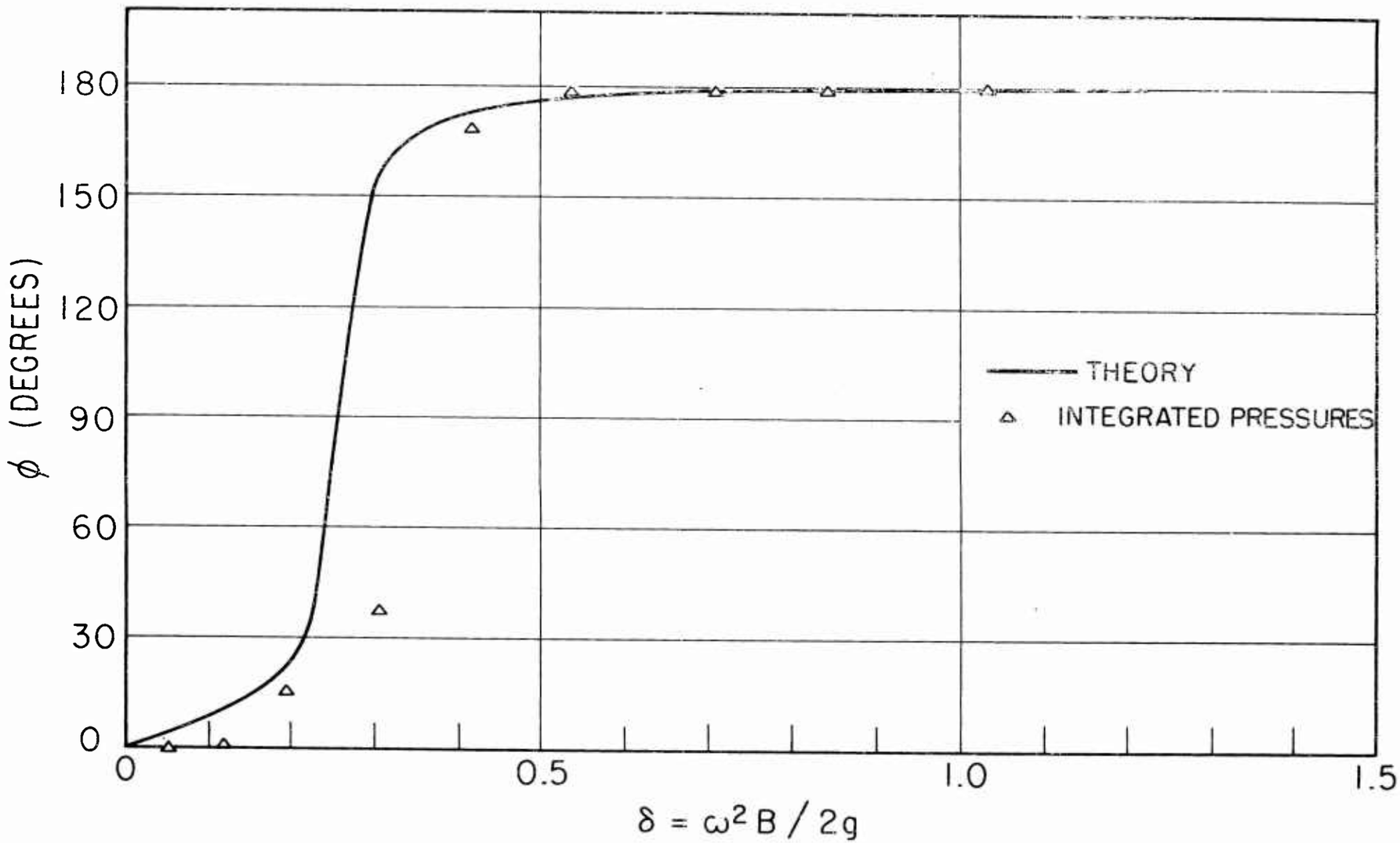

FIG. 37 FORCE PHASE ANGLE, ϕ, vs δ FOR MODEL 4